ADAPTIVE DETECTION OF BETA BURSTS OF LOCAL FIELD POTENTIALS RECORDED FROM SUBTHALAMIC NUCLEUS IN PATIENTS WITH PARKINSON'S DISEASE

by
Stephanie Velasco

A thesis submitted to the Biomedical Engineering Department,
Cullen College of Engineering
in partial fulfillment of the requirements for the degree of

MASTER OF SCIENCES

In Biomedical Engineering

Chair of Committee: Dr. Nuri F. Ince

Committee Member: Dr. Yingchun Zhang

Committee Member: Dr. Ashwin Viswanathan

University of Houston
August 2020

DEDICATION

To God.

My strong faith in him has helped me achieve goals that, at some point in my life, seemed impossible.

To my parents, Jose Ricardo Velasco and Rosalba Velasco.

I know that without you, this would not have been possible. Thank you for the tremendous support, and for the wise words that helped me move forward throughout my entire life.

Two of My Favorite Quotes:

“IT’S SUPPOSED TO BE HARD. IF IT WASN’T HARD, EVERYONE WOULD DO IT. THE HARD IS WHAT MAKES IT GREAT.”

-Tom Hanks, *A LEAGUE OF THEIR OWN*

“IT ALWAYS SEEMS IMPOSSIBLE UNTIL IT’S DONE.”

-Nelson Mandela

ACKNOWLEDGMENTS

I wanted to thank all the patients that took part in the research, because without their cooperation this research would not have been possible. I would like to express my special gratitude and thanks to my advisor Dr. Nuri F. Ince for his patience, guidance, and useful critique of my work. I also am grateful to Dr. Yingchun Zhang and the rest of my committee members; their expertise has been insightful and has helped enrich my work. I am thankful to Dr. Aviva Abosch for recording the data with the help of Dr. Nuri F. Ince at the Fairview Hospital of University of Minnesota. My sincere thanks also go to Dr. Ashwin Viswanathan for allowing me to be a part of a great PD clinical team. I am also thankful to the members of the Clinical Neural Engineering Lab, for always being so kind and generous. Last but not least, I wish to thank my beloved husband, Andrew, for always putting a smile on my face and for all the encouragement, support, and help that you have given me.

ABSTRACT

Parkinson's Disease (PD) affects 1% of the world population, with this number expected to increase within the following years. Local field potentials (LFPs) recorded from deep brain stimulation (DBS) leads placed into the motor territory of the subthalamic nucleus (STN) can be used to investigate the mechanism of PD and allows for further development of new therapeutic strategies. Beta band activity, which typically presents itself as bursts, has been continuously found in the LFP recordings of PD patients. These oscillations of neural activity have been shown to correlate with motor impairment and can be suppressed by dopaminergic medication and stimulation of the brain. A novel adaptive technique we developed uses local cosine packets to detect beta bursts in LFPs and segments the data appropriately using nondyadic segmentation. We show that the spectral entropy of these adaptively captured bursts previse patient symptoms accurately and may outperform the basic beta suppression approach, such as thresholding.

In this work, 120s of LFP data recorded in the resting state from chronic DBS leads of nine PD patients were segmented adaptively by entropy minimization. Using the recently developed algorithm, we performed the following: (i) adaptively segment STN LFP recordings into segments of 125ms or multiples of it, (ii) determine the entropy distribution of different time windows, (iii) correlate the change in entropy between unmedicated (OFF) and medicated (ON) states in different time windows with Unified Parkison's Disease Rating Scale (UPDRS) and computer-based measurements of bradykinesia. We found that as segment size increased, the difference in entropy between OFF and ON states enlarged. Based on entropy distribution, it was possible to determine whether a patient improved after the administration of medication. Similarly, the change of entropy in segments ≥375ms was highly correlated with the UPDRS and keyboard scores. These findings suggest that beta bursts can be adaptively segmented

without the use of a predetermined threshold, therefore allowing for robust quantification of disease severity. This could enable future closed-loop DBS algorithms to become more efficient and effective when stimulating based on beta bursts detection.

TABLE OF CONTENTS

LIST OF TABLES

LIST OF FIGURES

CHAPTER I

INTRODUCTION

1.1 Motivations and Specific Aims

Identification neurobiomarkers of PD and their use for the development of new treatment technologies gained a significant interest in the past decade [Bouthour et al., 2019; Tinkhauser et al., 2017]. As of now PD remains incurable, but fortunately there are treatment options available to help alleviate associated symptoms. The administration of dopaminergic medication and deep brain stimulation (DBS) are the most favorable treatment options [Fang and Tolleson, 2017]. Implanted DBS electrodes are typically used to suppress excessive beta activity in advanced cases of PD [Eusebio et al., 2012]. The electrodes can also be used to record LFPs from the subthalamic nucleus (STN) of the patients. The LFP recordings of PD patients have continuously presented bursting beta-band activity [Wichmann et al., 2011]; therefore, continuous brain stimulation is required to subside symptom impairment. Ultimately, automatic and reliable detection of these beta bursts in LFP recordings can improve novel therapies such as closed-loop deep brain stimulation.

In this study, we aimed to detect beta bursts adaptively using nondyadic time-frequency segmentations and investigate the correlation of burst-entropy with motor symptoms of PD. The LFP data analyzed was recorded continuously for 24 hours using chronic DBS electrodes from nine PD patients. Levodopa was administered to the patients three times, and their neural activity was recorded while ON and OFF the medication. During the ON and OFF states, the patients were instructed to rest for an extended time and were then asked to complete several tasks to quantify their improvement.

The nondyadic segmentation algorithm we developed analyzed the resting state LFP recordings to capture beta bursts and segment the recordings based on time-varying characteristics of the signal. We computed the power spectra of LFP in constructed segments and used entropy as a measure to quantify the sharpness of the spectrum in each segment. We investigated whether or not the entropy modulated by the adaptively captured beta-bursts can describe the differences in symptoms of OFF and ON medication states. We also characterized the time-frequency dynamics and power spectrum in the analyzed resting states.

1.2 Thesis Organization

This thesis is organized in the following way; the first chapter serves as an introduction to the primary purpose of this work and organization. The second chapter provides a background for PD, DBS, and LFPs. The third chapter introduces the methods used to analyze the data, and the fourth chapter demonstrates the results acquired. Finally, the fifth chapter is the discussion and presents future steps regarding the algorithm.

CHAPTER II

BACKGROUND

2.1 Parkinson's Disease

PD is an extremely complicated neurological disease that affects multiple neurological circuits. It degenerates dopaminergic neurons in the substantia nigra pars compacta (SNc), which, in return, causes the loss of dopamine in the striatum [Wichmann et al., 2011]. Initially, this disease was medically described as a neurological syndrome by Doctor James Parkinson [Parkinson, 1969]. He would refer to it as 'shaking palsy', and it was not until much later that this disease was redefined due to the findings of Jean-Martin Charcot [Goedert and Compston, 2017]. PD is the second most common age-related neurodegenerative disease, affecting people older than 60 years of age, after Alzheimer's Disease [Reeve et al., 2014]. Also, although it is not common for younger adults to suffer from PD, early onset can occur [Reeve et al., 2014]. This disease mostly affects the male gender, but women can be affected as well. It is estimated that about 10 million people worldwide are affected by this disease, and in the United States alone, there are 60,000 cases reported each year, which does not reflect the number of cases that go undetected [Naqvi, 2018]. PD affects not only the person's health but also lessens their quality of

life due to the symptoms the patient experiences, making it difficult to complete daily tasks and, over time, causing the loss of independence. Unfortunately, the root cause of PD is still unknown, and there are no known measures that can help prevent it.

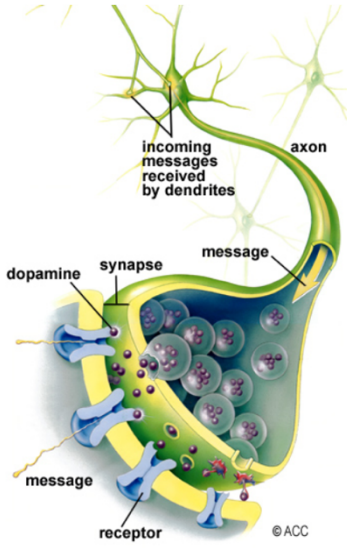

Figure 2. 1: Depicts the functionality of a healthy neuron. Reproduced from Mayfield Brain and Spine [2018].

To understand how PD works, understanding the basics of how a healthy neuron (Figure 2.1) communicates with the rest of the body is essential [Mayfield Brain and Spine, 2018]. Neurons are the basic building blocks of the nervous system. The structure of a neuron consists of the soma, axon, dendrites, and synapses. Dendrites, which are a tree-like structure, receive electrical impulses sent from other neurons. Afterward, these electrical signals received by the neuron causes electrical changes in the cell body, also known as the soma. Once all the information has been gathered, regeneration of the electrical impulse takes place at the axon hillock. Depending on the strength of the electrical impulse, the signal will then be carried down by the axon. The axon conducts electrical impulses away from the cell body to communicate with the rest of the neurons. These synapses are the junctions that help transmit the messages between the neurons. These synapses consist of one neurotransmitter; neurotransmitters would be what allows electrical impulses to cross from one neuron to another. Lastly, chemicals called monoamine oxidase-B (MAO-B) and catechol-O-methyltransferase (COMT) breakdown leftover neurotransmitters in the synapse, so it is clean and ready for the next impulse allowing the cycle to begin all over again [Mayfield Brain and Spine, 2018].

The basal ganglia-thalamocortical circuit's primary function is to provide motor control, such as prohibiting movements that would affect a smooth fluid motion when reaching for an object. A few other responsibilities of the basal ganglia would be learning, ocular-motor functions, and emotions. The basal ganglia is composed up of multiple subcortical-nuclei located within the brain. The group of nuclei that make up the basal ganglia is the substantia nigra (SN), subthalamic nucleus (STN), palladium, and striatum. The striatum is the most massive structure in the basal ganglia, and it consists of two separate nuclei structures, caudate nucleus and the putamen. The SN, name as such because of its high level of neural melanin, is composed of the SN pars reticulata (SNr) and SN pars compacta (SNc). Additionally, globus pallidus external (GPe), globus pallidus internal (GPi), and ventral palladium (VP) make up the palladium.

The basal ganglia controls body movements with a complex chain of neurons using an interconnected group of nerve cells [Mayfield Brain and Spine, 2018]. Initiations and executions of body movements start with the basal ganglia receiving neural input from the motor cortex regarding the initiation of movement. Afterward, the basal ganglia will deliver the message to the thalamus which would then send it to the motor cortex. Once at the motor cortex, the electrical impulse will then be sent to the muscle to execute the movement. These brain structures play a crucial role in what is known as the basal ganglia-thalamocortical circuit, and it is where the root of PD lies.

In a normal functioning basal ganglia-thalamocortical circuit, the SNc releases dopamine receptor subtypes, D1 and D2, into the putamen. D1 dopamine subtype excites neurons, which increases the activity in the direct pathway (Figure 2.2). D2 dopamine subtype will then inhibit the neuron activity in the indirect pathway, making it less likely to fire, resulting in smooth execution of voluntary movement. In PD this does not occur; the person will experience an

imbalance of D1and D2 release because of the degeneration of dopaminergic neurons. Therefore, this imbalance will generate an overactivity in the indirect pathway and an under-activity in the direct pathway, causing the symptoms which are associated with this disease.

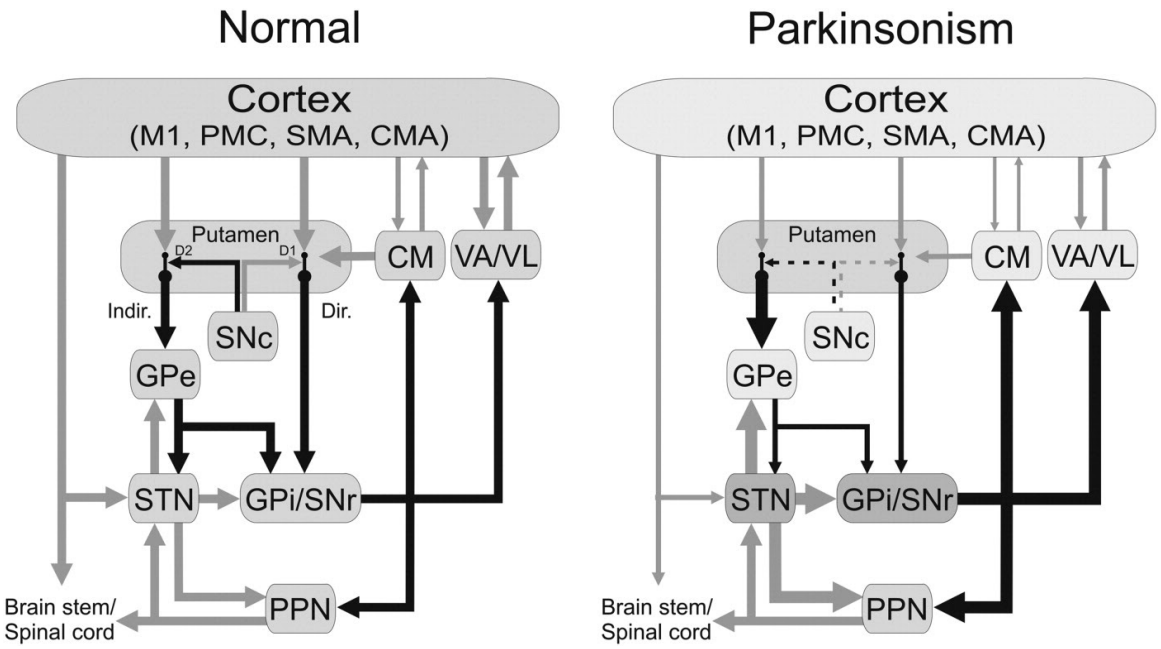

Figure 2. 2: Normal functioning basal ganglia-thalamocortical motor circuit (left) vs. Parkinsonian basal ganglia-thalamocortical motor circuit on (right). The black arrows represent inhibitory connections, and the gray arrows represent excitatory connections. The width of the arrows represents their activity. Reprinted from Galvan and Wichman [2008].

2.1.1 Symptoms

Patients who suffer from PD experience, but are not restricted to the following symptoms, such as rigidity, bradykinesia, akinesia, and rest tremor. However, patients will experience PD symptoms after the death of 80% of the dopaminergic neurons [Mayfield Brain and Spine, 2018].

Rest tremor is defined as a slow, involuntary, and rhythmic movement within the frequency range of 4-6Hz, which occurs when the person remains at rest [Jankovic, 2008]. It usually begins on one hand, foot or leg, and over time it slowly takes over other parts of the

body. Some patients can also experience rest tremor in the jaw, chin, mouth and/or tongue, making it challenging to communicate effectively with others.

Bradykinesia refers to the slow movement PD patients may experience, while akinesia refers to the reduced ability to initiate movement. Both symptoms play a part in the difficulty of postural instability. At the onset stage of the disease, the person may first experience difficulty in swinging their arms when moving. As the disease progresses, they may experience slowness in walking while making it difficult to take more substantial steps.

Rigidity is one of the symptoms of PD that causes pain because of the muscle stiffness that occurs. Frequently, patients will experience shoulder pain, and sometimes it may be diagnosed by physicians as arthritis, bursitis or rotator cut off injury due to the similarities. Although misdiagnosis does occur, these symptoms are one of the most frequent manifestations of PD [Jankovic, 2008]. Patients can experience a few other symptoms when suffering from PD, such as depression, cramped handwriting, shuffling gait, and sleep disorders.

PD symptoms severity can be quantified using the Unified Parkinson's Disease Rating Scale (UPDRS). UPDRS was developed in the 1980s and was later modified by MDS, therefore allowing evaluations of motor and non-motor symptoms associated with the disease [Goetz et al., 2008]. UPDRS consists of 4 parts, part 1 evaluates mentation, behavior, and mood, part 2 evaluates activities of daily life, part 3 completes a motor examination, and part 4 rates complication of therapy [Perlmutter, 2009]. Each subcategory is rated on a scale from 0 to 4, 0 being normal (no impairment), and 4 being severe impairment.

2.1.2 Diagnosis

Since there are no current tests available to detect PD, it may become difficult to diagnose due to symptoms being similar to other diseases, and not everyone affected experiences the same symptoms. Fortunately, physicians are required to make a thorough examination of the patients' medical history, and a physical exam is needed to diagnose the patient with PD accurately.

2.1.3 Treatments

The current treatment options available cannot cure PD, but they can help alleviate mild to moderate symptoms. Although just like other medications, symptom relief dissipates over time, and in some cases the patient may experience side effects. Levodopa, also known as L-3,4-dihydroxyphenylalanine, or L-DOPA, is an effective dopamine replacement agent treatment for PD. L-DOPA crosses the blood-brain barrier through an amino acid transporter, and a decarboxylase enzyme will convert it into dopamine in the dopaminergic neurons. However, only 5% to 10% of the administered levodopa crosses the blood-brain barrier, and the remaining part has to be metabolized elsewhere [Meloni et al., 2015]. The rest of the medication may be metabolized either in the bloodstream or after it is converted to dopamine. L-DOPA is usually administered with a CMOT blocking agent to prevent further metabolization of the medication when not necessary, therefore reducing the chances of liver toxicity. Therapeutic dose of L-DOPA will vary depending on the patient, and a vast majority of patients typically respond well to doses of 300-600 milligrams per day [Salat and Tolosa, 2013].

Even though other options are available, L-DOPA is known to be effective in reducing rest tremor and other symptoms in PD patients. Usually, the effects of the medication last for

several hours before it wears off, and symptoms resurface. Unfortunately, when taking L-DOPA over a lengthy period, patients can experience L-DOPA induced dyskinesia. However, a combination of L-DOPA and DBS can help reduce dosage quantity and medication side effects.

2.2 Deep Brain Stimulation

A better understanding of PD allowed for significantly improved techniques; thus, surgeons first revisited the use of ablative procedures [Whichmann and DeLong, 2006]. However, over the last century, the surgical treatment of PD has evolved from an ablation with careful placement of lesions within a variety of brain structures into stimulation of particular brain targets within the basal ganglia subregions [Wagle and Okun 2014]. DBS delivers rectangular electrical impulses to targeted regions of the brain. Stimulation is typically applied in the STN or GPi (Figure 2.3) to reduce symptoms since there has been extensive evidence showing that abnormally synchronized activity in the beta band has been principally found in these brain structures [Eusebio et al., 2012]. DBS electrodes are placed on one or both sides of the brain, and stimulation parameters are fine-tuned to each individual's need. The physician programmer can select lead contacts (positive, negative, or off—in any combination), stimulation mode (bipolar or monopolar with the INS case positive), and stimulation parameters (amplitude, 0–10.5 V in 0.1-V steps; rate, 66 steps from 3 to 250 Hz; PW, 60–450 ms in 30-ms increments; and on/off cycling from seconds to 24 h on/off per day) [Coffey, 2009].

Stimulation of the STN at a higher frequency has helped subside most symptoms for patients by preventing neurons from firing and therefore removes the excessive inhibition from the indirect pathway. As time passed, DBS of the STN became more frequent, since methods

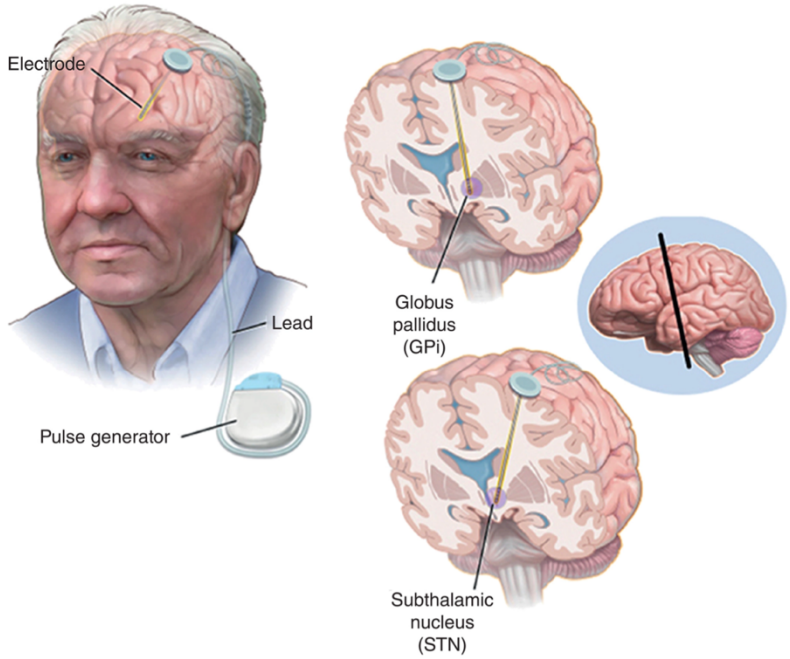

Figure 2. 3: Schematic for deep brain stimulation leads implantation and hardware required. DBS leads can be placed either in the STN or GPi (most common for PD patients). The pulse generator can be fine-tuned to the individual's needs. Adapted from Hickey and Stacy [2016]

for implantation grew to be more precise and effective. There are a variety of placement techniques used to help map the optimal area for the DBS electrode (Figure 2.4). Placing the electrodes in the wrong location will reduce the efficiency of the stimulation and will lessen the probability of providing patients with relief; this leads to several side effects such as loss of cerebrospinal fluid, or pneumocephalus, among other complications. On the day of surgery, the external part of the head is numbed, and a head frame is placed on the head of the patient. At this point, the patient will/can experience a pressure sensation, but the pain should not be present. Pre-operatively (Pre-OP), an MRI or CT is taken, and a frame-based stereotaxy system is used to obtain the Cartesian coordinates of the frame. Afterward, the frame is adjusted to the corresponding coordinates, and microelectrodes are placed inside a cannula so they can be

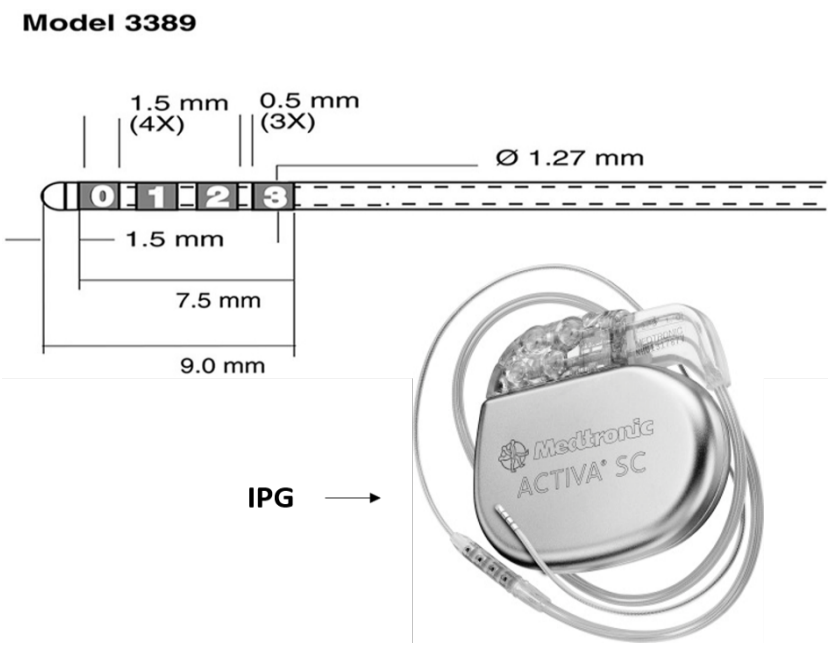

Figure 2. 4: Medtronic DBS lead (model #3389) schematic shown at the top left. Medtronic IPG device with DBS electrode shown in the bottom right. Image adapted from Darvas and Hebb [2014] and https://doi.org/10.1016/B978-0-12-805353-9.00076-0

inserted into the brain using an electrode guiding system. Microelectrodes can be used to obtain Pre-OP LFP recordings and to help locate the best implantation location of DBS macroelectrodes for optimal programming. Although, in most cases, more than one technique is used for the certainty of DBS electrode placement. Afterward, the depth of the tissue is usually determined by using ventriculography, CT, and MRI to verify electrode placement location. Intraoperative testing is also completed to test the side effects the patient may experience when the electrode is stimulating at a specific location. One goal during surgery would be to achieve the most favorable electrode placement without inducing side effects.

However, even though stimulation can help subside most of the symptoms, DBS cannot treat postural instability. Particular symptoms may not respond to dopaminergic medication, indicating they are possibly controlled by a neural pathway that differs from the dopamine-dependent pathways responsible for tremulous/anti-kinetic symptoms of PD [Thompson et al.,

2014]. Requiring the physician to make an extensive evaluation of the patient before they can be considered as a DBS candidate and undergo surgery. Therefore, an ideal candidate will have PD, responds to their dopaminergic medication, and will not have untreated severe depression or dementia. Ultimately, the patient's reaction while on medication would be the best indication of whether DBS will work for them.

However, this treatment option comes with drawbacks, since conventional DBS stimulates the brain continuously it can induce side effects on the patient. Reason being that it is not possible to predict when a patient will experience PD symptoms to stimulate only when they occur.

2.3 Local Field Potentials

DBS macroelectrodes implanted are required to be left in the brain over a long time to aid with symptom relief. Although the primary purpose of DBS macroelectrodes is stimulation, LFPs may be recorded directly from DBS-electrodes in the few days that follow implantation while externalizing of leads occur before connection to the subcutaneous stimulator [Brown and Williams, 2005]. LFP recordings give us access to a measurable synchronous activity occurring in particular parts of the brain. When using standard analytic methods, the characteristics of LFP recordings can be studied, which in return can help translate what is occurring in the human brain.

When electrodes are placed in the brain for an extended time, impedance becomes a significant factor to keep into consideration when recording or stimulating. Generally, LFP recording is done before the IPG implantation to obtain optimal recordings. However, recordings can be done up to days or years later without affecting the quality of the signal. A recent study

tested the quality of LFP recordings during different stages of the surgery and after several years. The LFPs were recorded from the DBS electrodes, and electrode encapsulation was observed over a long time. Although some changes occurred during, they determined it was possible to obtain good quality LFP recordings even after several years had passed [Abosch et al., 2012].

2.3.1 Local Field Potentials Recorded from the STN of a PD Patient

In recent research studies, LFPs recorded from the STN have been used for target localization and to determine medication onset. These studies suggest that the exaggerated activity of the beta band (13-35 Hz) in the basal ganglia is a hallmark for patients with PD [Tinkhauser et al., 2018]. Furthermore, most beta oscillatory cells were also found towards the dorsal part of the STN [Wichmann et al., 2011]. Additionally, PD rigidity has shown to correlate with the power of beta oscillations (13 -30Hz) [Thompson et al., 2014]. Typically, during the OFF state, a frequency peak within the beta range is present in the power spectra (Figure 2.5C). However, the beta peak will sometimes translate to a 70Hz peak in the ON state, as seen in the LFP recording in Figure 2.5D. Gamma and High-Frequency Oscillation above 200 Hz band powers increase after the administration of L-DOPA, caused by the contribution of a higher frequency signal to symptomatic improvement. Therefore, suggesting that gamma activity is prokinetic since it promotes normal, voluntary movement [Thompson et al., 2014]. The initiation of voluntary movement causes the suppression of beta-band, and it is associated with event-related desynchronization (ERD). Therefore, termination of voluntary movement promotes event-related synchronization (ERS), causing beta-band power to decrease. Some studies suggest that PD patients experience symptoms because of pathological synchronization at low frequencies (13 – 35 Hz) [Eusebio et al., 2012]. An increase in local and interhemispheric synchronization is related to the cause of beta bursts in PD patients [Tinkhauser et al., 2017].

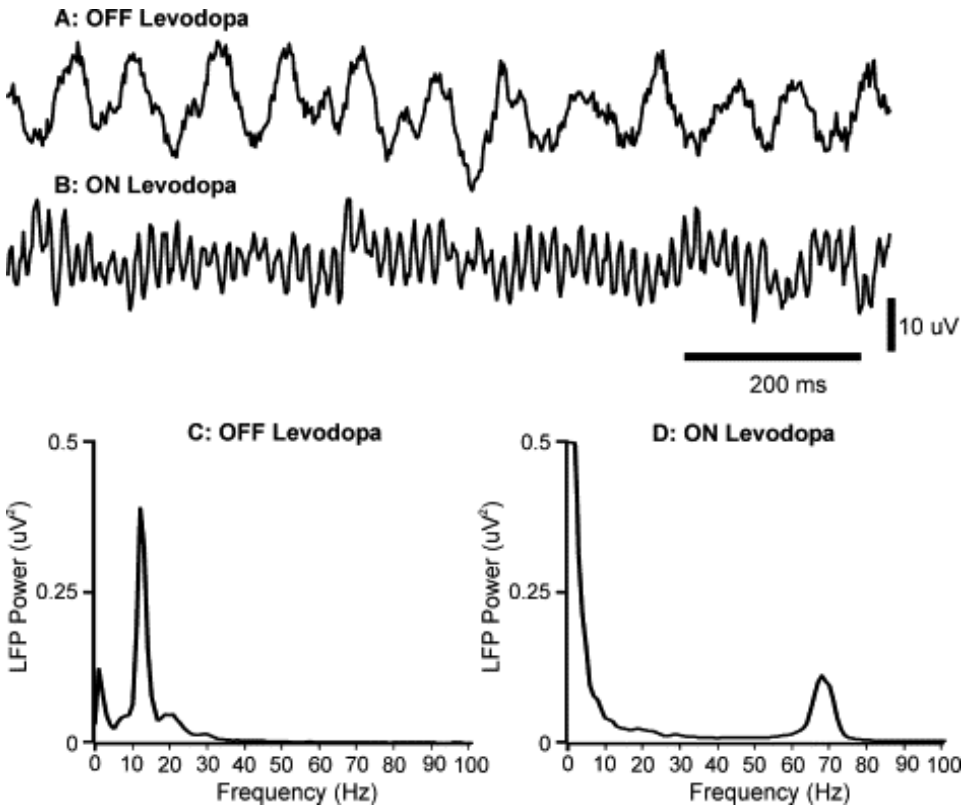

Figure 2. 5: A) and B) depicts the LFP activity of a patient during the OFF and ON medication state. C) and D) show the power spectra of the corresponding LFP recordings. Reproduced from Brown and Williams [2005].

Therefore, suggesting that dopamine depletion causes highly synchronous beta activity [Thompson et al., 2014]. It is suspected that this excessive synchronization within and in the basal ganglia is what contributes to clinical impairment. The correlation of beta-band power suppression induced by levodopa with the improvement of clinical impairment was ($r = 0.811, P < 0.001$), which strengthens the hypothesis of beta-band promoting clinical impairment (Figure 2. 6) [Kuhn et al., 2006]. Moreover, low-beta power was also correlated ($r = 0.5, P = 0.03$) with keyboard improvement ratio [Ozturk et al., 2019]. Additionally, previous studies had reported patient symptoms were diminished when stimulation was applied at the exact location where beta-band activity was at its highest (Figure 2.7) [Eusebio et al., 2012].

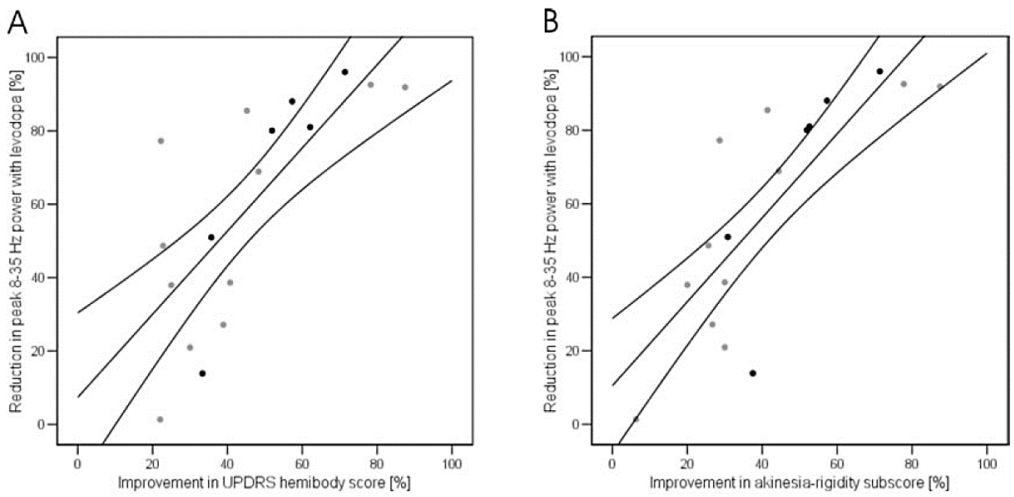

Figure 2. 6: A) The scatter plots show the correlation ($r = 0.811,\ P < 0.001$) between reduction in beta peak with levodopa and improvement of UPRS hemibody subscore. B) Scatter plots the correlation between the reduction in beta peak power and improvement of akinesia-rigidity subscore ($r = 0.835,\ P < 0.001$). Adapted from Kuhn et al. [2006].

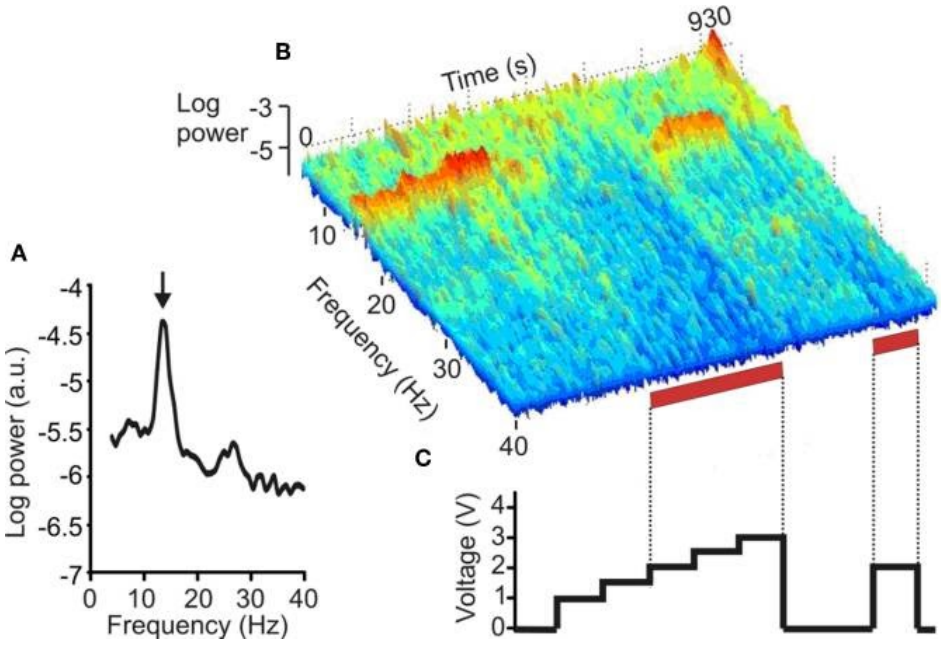

Figure 2. 7: A) LFP Power spectrum prior to stimulation. B) Beta band suppressed once DBS was applied, which is denoted by red bars. C) Depicts how much voltage of DBS was applied as time progressed. Adapted from Eusebio et al. [2011].

2.3.2 Beta Bursts

The activity in the beta band fluctuates over time and appears as bursts with large amplitudes. Thus, making it difficult to predict its appearance since it is random, has different durations, and amplitudes. Being the reason to why continuous stimulation of the brain is required for complicated cases of PD and, most recently, adaptive deep brain stimulation methods are being studied. In a recent adaptive deep brain stimulation study, a predetermined threshold was used to detect beta bursts that were ≥ 100 ms (Figure 2.8A); they effectively stimulated when beta bursts were detected, therefore reducing the number of large high amplitude bursts [Tinkhauser et al., 2017]. Both beta bursts duration and phase-amplitude coupling have emerged as more selective biomarkers than beta band power itself, and they could potentially be used as a feedback signal in closed-loop DBS [Bouthour et al., 2019]. Beta bursts are continuously positively correlated with muscle rigidity, and bradykinesia suggesting that it may have a mechanistic role. In the OFF state, beta bursts are frequent and have a longer duration. Fortunately for most patients, exaggerated beta bursts activity and beta-band power can be suppressed with the administration of L-DOPA.

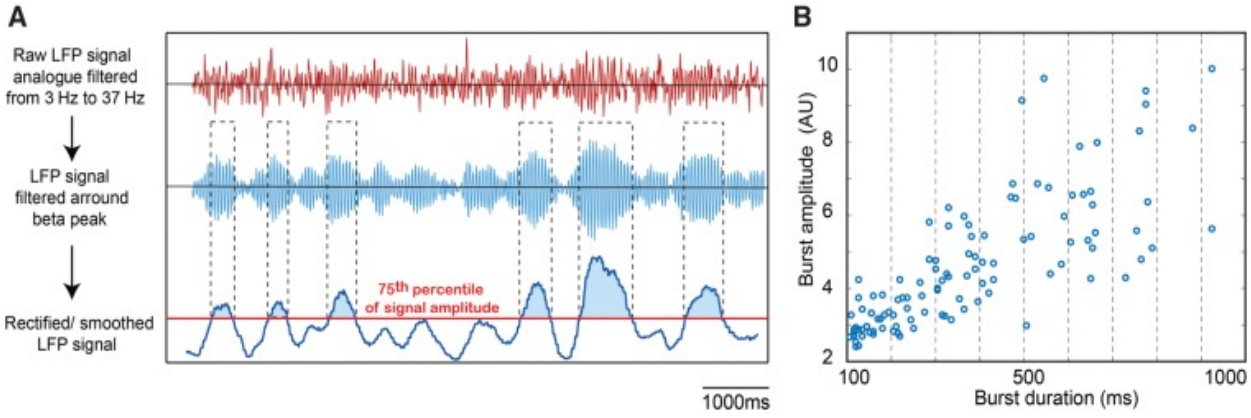

Figure 2. 8: A) A threshold method was used to detect burst with a length of 100 ms and greater. The LFP data was filtered to around each individual's beta peak. B) Demonstrates how the amplitude of beta bursts increases as burst duration increases. Adapted from Tinkhauser et al. [2017].

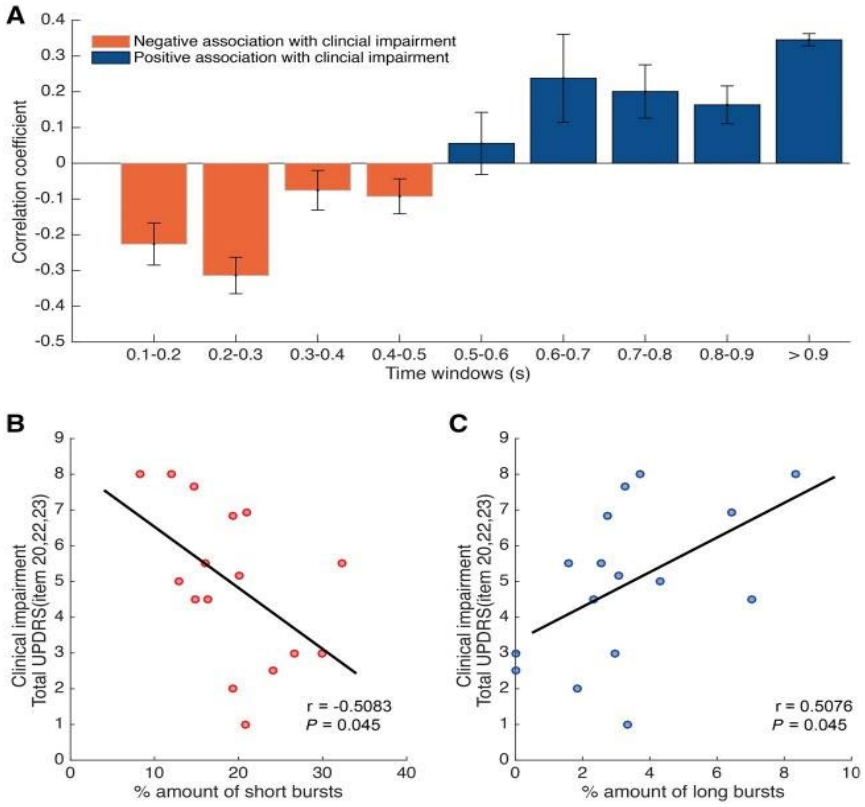

Figure 2. 9: Depicts the correlation between long and short bursts with clinical impairment. A) shows the distribution of bursts with respect to their length. B) Negatively Correlates shorts bursts with clinical impairment. C) Positively correlates long bursts with clinical impairment. Reproduced from Thinkhauser et al. [2017].

L-DOPA modifies the delivery of beta bursts by making them less frequent and shortening the burst period. As a result, burst amplitude and duration decreases (Figure 2.8B) and prevents symptoms from surfacing, until the medication wears off. Due to this response, beta bursts with longer duration have a positive correlation ($r = 0.5\,, P = 0.045$) with clinical impairment, while shorter bursts a negative correlation ($r = -0.5, P = 0.45$) with clinical impairment (Figure 2.9) [Tinkhauser et al., 2017]. While in the ON state, suppression of slower oscillatory signals occurs, and the imbalance of the dopamine subtypes are restored. However, in some cases, beta-suppression by medication may not happen, and it is due to beta-band having two subcategories, low beta (8 -20Hz), and high beta (21-40Hz). The depletion of dopamine in the substantia nigra

pars compacta causes the activity of the low-beta band, making it pathological. While high-beta band activity is physiological.

CHAPTER III

METHODS AND DATA

3.1 METHODS

We are proposing dyadic and nondyadic segmentation methods of the LFP in the time axis for the adaptive detection of beta bursts. We use Local Cosine Packets (LCP) to construct time segmentations, adapting the time-varying characteristics of the LFP signal. We anticipate that excessive beta activity or beta bursts that occur randomly with varying duration can be captured by dividing LFP signals into segments that are proportional to the duration of these oscillations. Our hypothesis is that the entropy of the power spectrum of the beta bursts estimated from adaptive segmentations can be a better predictor of the motor symptoms and their improvement following dopaminergic medication. In this scheme, first, we employ the best basis algorithm constructing such segments over a dyadic tree structure. Later we improve this method with nondyadic segmentation for isolation of beta bursts, which do not necessarily appear in dyadic segments. In particular, the LFP recordings are rapidly segmented from left to right by minimizing the entropy of LCP estimated in adjacent windows in an iterative fashion. We compute time-frequency maps of LFP in these adapted windows to visualize the change of frequency throughout the segments as time progresses. Afterward, the entropy of each segment

was computed to be used as a feature to characterize the sharpness of the spectrum and later predict the improvement in symptoms of the PD patients. Below we first describe the adaptive time segmentation methods and later use the entropy of the spectrum in these windows to obtain the difference in entropy between OFF and ON medication states and correlate it to UPDRS and keyboard scores.

3.1.1 Local Cosine Packets

3.1.1.1 Discrete Cosine Transform Type IV

To represent the time-varying spectrum of neural activity, the signal is generally divided into disjoint fixed length rectangular windows and analyzed with Fourier bases. This method has two drawbacks. First, fixed window length provided uniform frequency resolution and did not adapt the time-varying properties of the signal. Second, multiplying a signal with a rectangular window causes side lobe artifacts, which extend to high frequencies. To avoid these artifacts, smooth windows are preferred. However, when smooth windows are used, then orthogonality is lost when Fourier bases are used.

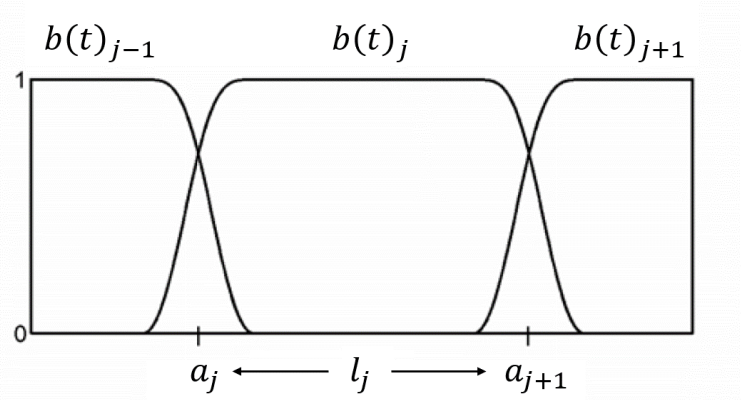

Figure 3. 1: Smooth windows used, which also overlap with its neighbor intervals

It has been shown that one can construct orthogonal bases by using smooth windows modulated by cosine IV basis. This transform is also named as the lapped orthogonal transform or local

cosine packets. The windows are not only smooth, but they also overlap their neighbor interval (Figure 3.1). Despite the overlap, DCT-IV serves as an orthonormal basis and can be effectively used to study the local spectrum of the signal. Therefore, local cosine packets can be used to expand a signal and provide local spectral representation with minimal spectral leakage due to the use of smooth windows. The discrete cosine transform can decompose a signal into the sum of cosines which oscillate at different frequencies. This transform results in real integer values to represent a discrete-time signal in the frequency domain.

Hence a signal, $s(t) \in L^2$, could be written as terms of the functions $\psi_j^k(t)$ as equation 3.1 and

$$s(t) = \sum_{j \in Z, k \in N} p_k^j \psi_k^j(t) \tag{3.1}$$

can be rearranged as $p_k^j = s(t) \cdot \psi_k^j(t)$, where p_k^j coefficients are calculated using DCT-IV with the following procedure [Wickerhauser et al., 1995; Ince et al., 2004]. Here, $\psi_k^j(t) = b_j(t) \frac{\sqrt{2}}{\sqrt{l_j}} cos \frac{\pi}{l_j}\left(k + \frac{1}{2}\right)(t - a_j),\ j \in Z,\ k \in N$ with $l_j = a_{j+1} - a_j$, being an orthonormal basis for $L^2(R)$ and $b_j(t)$ is the smooth window that overlaps with the windows next to it, as shown in Figure 3.1. These are satisfied by $b_{j-1}^2(t) + b_j^2(t) + b_{j+1}^2(t) = 1$ for $t \in [a_j - n, a_{j+1} n]$ where $n \leq \frac{l_j}{2}$ would be the length of the overlapping part, as shown in Figure 3.2A.

3.1.1.2 Best Basis Algorithm

Local cosine packets can be applied to obtain an adaptive time segmentation of a particular signal over a dyadic tree structure; the nodes of the tree represent a segment with

mother and child-relationships depicted in Fig 3.2. Simply the mother segment covers the same amount of duration of the union of its children. The signal is decomposed into local cosine packets in each sub-segment, thus providing localized characteristic details of the signal until the last layer of the tree structure is reached.

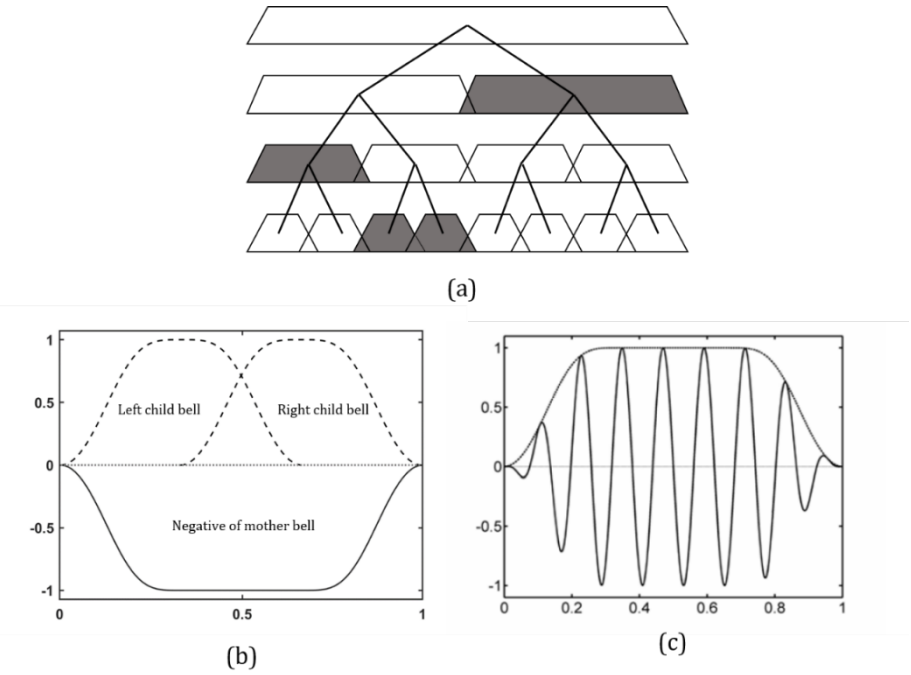

Figure 3. 2: a) Dyadic tree structure used, sub-segments represent a smooth window. b) Smooth windows of child bell and mother bells. c) Cosine packet with smooth window applied

The best basis (BB) method of Wickerhauser et al., 1992, employs an entropy minimization strategy over this dyadic tree to select the nodes that adapt to time-varying characteristics of the signal. Later, this method has been successfully extended to classification (local discriminant bases -LBD) applications to select the time-frequency representation tuned for discrimination [Saito et al., 2002]. The LDB method was also used in EEG classification [Ince et al., 2009; Ince et al., 2007] for a brain-machine interface. In dyadic adaptive segmentation, the partitions are selected from a dyadic-partitioning tree, and at each level, the

signal is divided into 2^j segments where j is the level, where the interval [a_j , a_{j+1}] describes a partition [Wickerhauser et al., 1992; Ince et al., 2004]. Therefore, all the data that was introduced into the algorithm needed to have a length, which was to the power of two. The algorithm is visually represented in Figure 3.2A, as the pruning processing of the dyadic tree begins from bottom to top. Local cosine packets mentioned in Section 3.1.1, were used to decompose the signal in each segment after a folding process took place, and the average of coefficients is obtained after time-shifting [Boulet, 2014]. This results in the estimation of the power spectra of the signal various segments with different resolutions in a redundant fashion. The best base algorithm was implemented to select the segments that adapt the time-varying characteristics of the signal through the minimization of the entropy cost function.

The BB method is outlined in three steps. First, the signal must be expanded into Cosine Packets in accordance with the tree structure. Secondly, after decomposing each segment into Cosine Packets, the cost function (the Shannon entropy) of each sub-segment is obtained

$$H_s = -\sum_{k=1}^{m} p_k^2 \log(p_k^2), \tag{3.2}$$

here p_k represents the DCT-IV coefficients in a particular segment normalized to the total energy of the signal. Here H_s estimates the sharpness of the spectrum.

Lastly, the pruning process takes place from bottom to top, thus allowing for minimization of entropy (Figure 3.3). Typically, this pruning works as such to compare the mother and children sub-segments. When the mother segment is has a lower cost function, this segment will be kept by disregarding the children segments. On the other hand, if the children sub-segments have lower entropy values combined, the mother's cost function will be replaced

with the child's entropy. After comparing with the upper level, if it determined that the children have lower entropy, the mothers will be discarded, and the children will be kept.

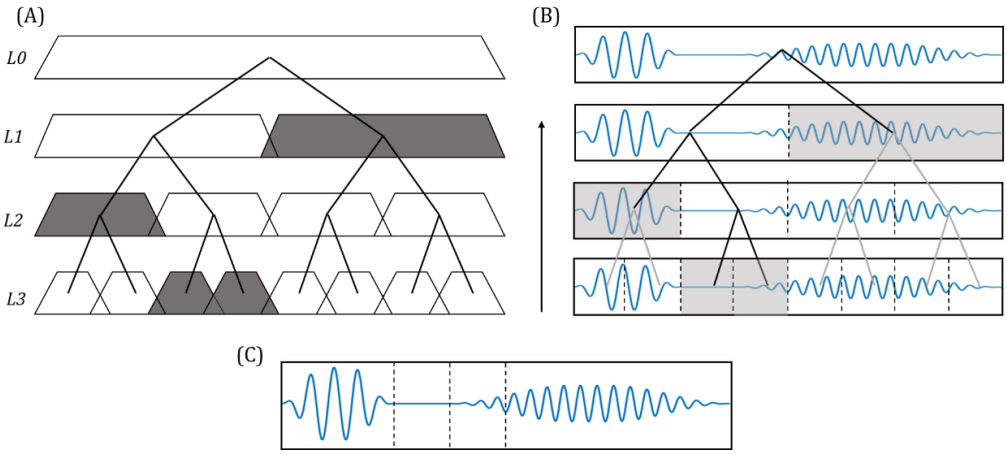

Figure 3. 3: A) Dyadic tree structure. B) Dyadic tree structure applied to a synthetic signal. C) Final segmentation for the synthetic signal

3.1.1.3 Nondyadic Segmentations

The BB of Wickerhauser and LDB method of Saito are selected over a dyadic tree by a divide and conquer algorithm. However, there is no guarantee that the local patterns will occur in dyadic segments. In case the localized events in the analyzed data do not match to the tree structure, then both algorithms result in arbitrary trees/segmentations. Therefore, a more flexible segmentation algorithm is desired.

Ince et al., 2006, proposed a nondyadic segmentation based on a Merge and Divide strategy for the discrimination (Figure 3.4). In this method, rather than employing a bottom to top cost function maximization search on a dyadic tree as done in LDB and BB methods, they merged consecutive segments based on the change of the cost function. Nondyadic segmentation is very similar to the dyadic segmentation method previously mentioned, but the difference lies in the technique used to segment the data. While dyadic segmentation prunes a tree from bottom

to top, the nondyadic algorithm segments data from left to right recursively. As depicted in Figure 3.4 from left to right, the consecutive segments are merged if the cost function (entropy) is minimized in the mother segment. Thus, this means that children are not necessarily half of the mother windows as it was in the dyadic segmentation. In the next iteration, the merged segment on the left becomes a child, and it is merged with the neighboring child window based on the change in the cost function. Consequently, the merged segments can be multiples of the finest segments. While Ince et al., 2006 used this approach to maximize discrimination in this study, we aimed to minimize the Shannon entropy of the spectrum to construct segments based on time-varying properties of the beta bursts.

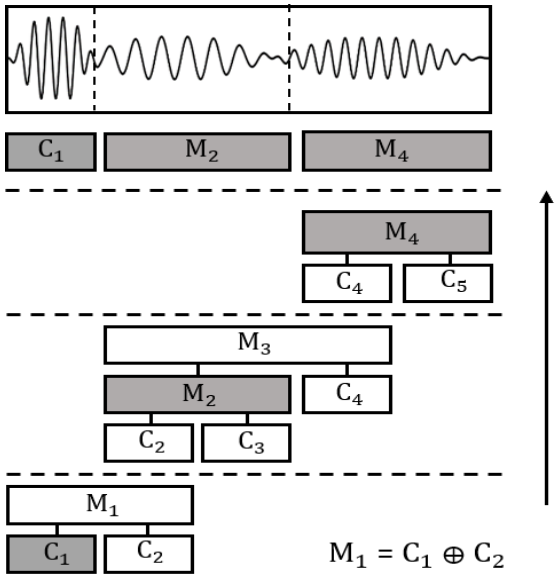

Figure 3. 4: A schematic demonstration of how a nondyadic algorithm segments data from left to right by comparing the entropy of adjacent segments. The first iteration starts at the bottom with the left-most segments (C1 and C2) and iterated until we reach the right-most segments of the data (C5).

One drawback when using this type of transform would be that it is not shift invariant. A phase delay in the original discrete-time signal will prompt unprecise computation of the coefficients, which will then result in an inaccurate representation of the signal in the frequency domain. However, imposing a time shifting signal operation help can help overcome this. This shifting procedure expands the data by generating its time shifted versions in both directions in a circular manner, known as a "spin cycle" procedure [Saito et al., 2002]. In this procedure, if the desired number of shifts is τ then the training set is expanded to $2\tau + 1$ including the original signal, and it shifts by $-\tau, -\tau + 1, \ldots, \tau$ [Ince et al., 2006].

3.1.2 Entropy of the Power Spectrum

Claude E. Shannon first introduced Shannon entropy in 1984, and it is now widely used in a variety of engineering applications. The Shannon entropy of a distribution is the expected amount of information from that event. Furthermore, Shannon entropy is the negative sum of the probability multiplied by the log of the probabilities. In our work, the normalized power spectrum of the LFP can be seen as the probability density function. Hence, the entropy measures the sharpness of the spectrum of the signal. For instance, if a signal is built up from a pure oscillation, here beta burst, it should have only a few DCT-IV coefficients, which are nonzero, resulting in a lower entropy. In case the signal is white noise, then the power spectrum is expected to be uniform resulting in a lager entropy, H_S.

Depending on the log function used, entropy can be computed in units of bits (binary units) when using log_2 or nats (natural units) when using log_{10}. However, in its original form, the entropy is sensitive to the signal length, and this can cause problems in comparison of segments with different lengths. Therefore, normalized entropy is used

$$H_s = -\sum_{i=1}^{m} \frac{p_i^2 \log(p_i^2)}{log(n)}, \tag{3.3}$$

when it is divided by $log(n)$, it results in $H_s \in [0,1]$. Where n is the length of the corresponding segment in samples. Normalized entropy was used to compare the entropy of segments that had varying lengths. Thus, allowing for a fair comparison. Another option would be to compute (Fast Fourier Transform) FFT coefficients using the same number of FFT points for all segments regardless of their length.

After we computed the entropy for different segments, we then weighted it based on the power of the segments

$$H_w = \frac{\sum_{k=1}^{n} H_{\mathrm{k}} \cdot w_{\mathrm{k}}}{\sum_{k=1}^{n} w_k}, \tag{3.6}$$

where H_k stands for the normalized entropy and w_k stands for the allocated weight value. We calculated weighted entropy to consider the varying power of the segments. This helped us determine the relative importance of segments, based on their power or other patterns that can be used as a weight factor. Here, in addition to the signal power, we also considered the ratio of low beta band power to high beta band power as a novel weight factor.

Additionally, we calculated the difference in entropy between the two states (OFF vs. ON)

$$\Delta H_w = H_w^{OFF} - H_w^{ON}, \tag{3.7}$$

where H_w^{OFF} stands for the weighed entropy value of the OFF-medication state and H_w^{ON} stands for the weighed entropy value of the ON-medication state. ΔH_w allows us to correlate mean weighted entropy of segments regardless of their length to UPDRS and keyboard scores. However, we can also calculate the difference in entropy by using normalized entropy instead of weighted entropy in equation 3.7. We then correlated differences in normalized entropy to clinical improvement for specific segment lengths; hence the need for weighted entropy is not necessary.

3.1.3 Correlation Coefficients

The correlation coefficients were calculated using Pearson correlation

$$\rho(x,y) = \frac{1}{n-1}\sum_{i=1}^{n}\left(\frac{x_i-\mu_x}{\sigma_x}\right)\left(\frac{y_i-\mu_y}{\sigma_y}\right), \tag{3.8}$$

where N is the sample size, x_i and y_i are the individual samples points, μ_x and μ_y are the means of x and y , and σ_x and σ_y are the standard deviations.

3.2 EXPERIMENTS WITH SYNTHETIC DATA

3.2.1 Adaptive Segmentation Algorithms with Synthetic Data

All of the following segmentation algorithms were written in MATLAB software (version R2018b; The Mathworks, Inc., Natick, Ma). Two test signals (Figure 3.5) of four second lengths were created to mimic beta bursts with varying frequencies and duration. Here we study time-varying characteristics of these test signals using constructed segmentations. Three different segmentation methods are studied:

1. Fixed windows of 125ms
2. Dyadic, with a finest level/segment length of 125ms
3. Nondyadic, with finest segment length being 125ms

Note, the smallest window used in all the algorithms was set to 0.125s, to accommodate the period of the lowest frequency of interest (8Hz). All the segmentation methods used the same time shifting technique [Saito et al., 2002; Ince et al., 2006]. With $\tau = 8$, decomposed the signal into local cosine packets and computed the spectral entropy. This experiment helped us determine the degree of effectiveness of each algorithm in localizing time-varying bursts through

entropy minimization. Thus, allowing a decision to be made on which approach to implement on real LFP data recorded from the STN of PD patients. Once segmentation was completed, FFT was computed in each constructed segment and normalized entropy was used to characterize the

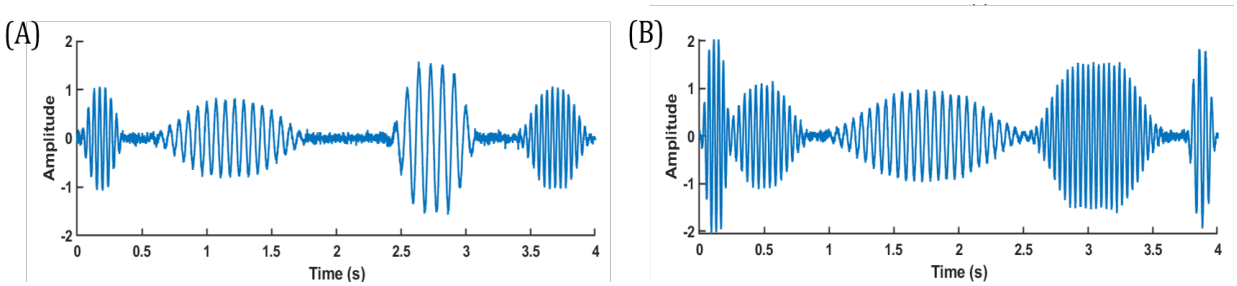

Figure 3. 5: The two different test signals were used to test the dyadic, nondyadic, and fixed segmentations. A) The signal is composed of background white noise, 23 Hz (0.375s), 14Hz (1s), 11Hz (0.75s), 24Hz (0.5s). B) The signal is composed of background white noise, 27Hz (0.25s), 23Hz (0.5s), 16Hz (1.5s), 25 Hz (1s), 21Hz (0.250s).

sharpness of the spectrum. Additionally, the entropy of segments was weighted based on their power. Finally, we used the total weighted entropy across segments to assess the effectiveness of each segmentation method.

Fixed segmentation was used as a baseline experiment to determine the effectiveness of the other two algorithms. The results are provided in Figure 3.6, along with the change in entropy. When fixed 0.125s long windows are used to segment the test signals, it provided uniform time-frequency resolution and larger entropy. As expected, using one uniform window size does not offer any advantage to the time-varying characteristic of the signal.

When introducing the test signals into the BB method, we noted that segments length became longer around beta bursts. Although a few artificial beta bursts were preserved, others were truncated in the middle due to the lack of segmentation flexibility.

We noted that the nondyadic algorithm provides the desired flexibility for segmenting LFP data. The synthetic bursts were captured, and not truncated as they were in dyadic

segmentation. When the total entropy estimated from each segmentation method is compared, we noted that nondyadic segments had the lowest entropy, followed by dyadic segments. As

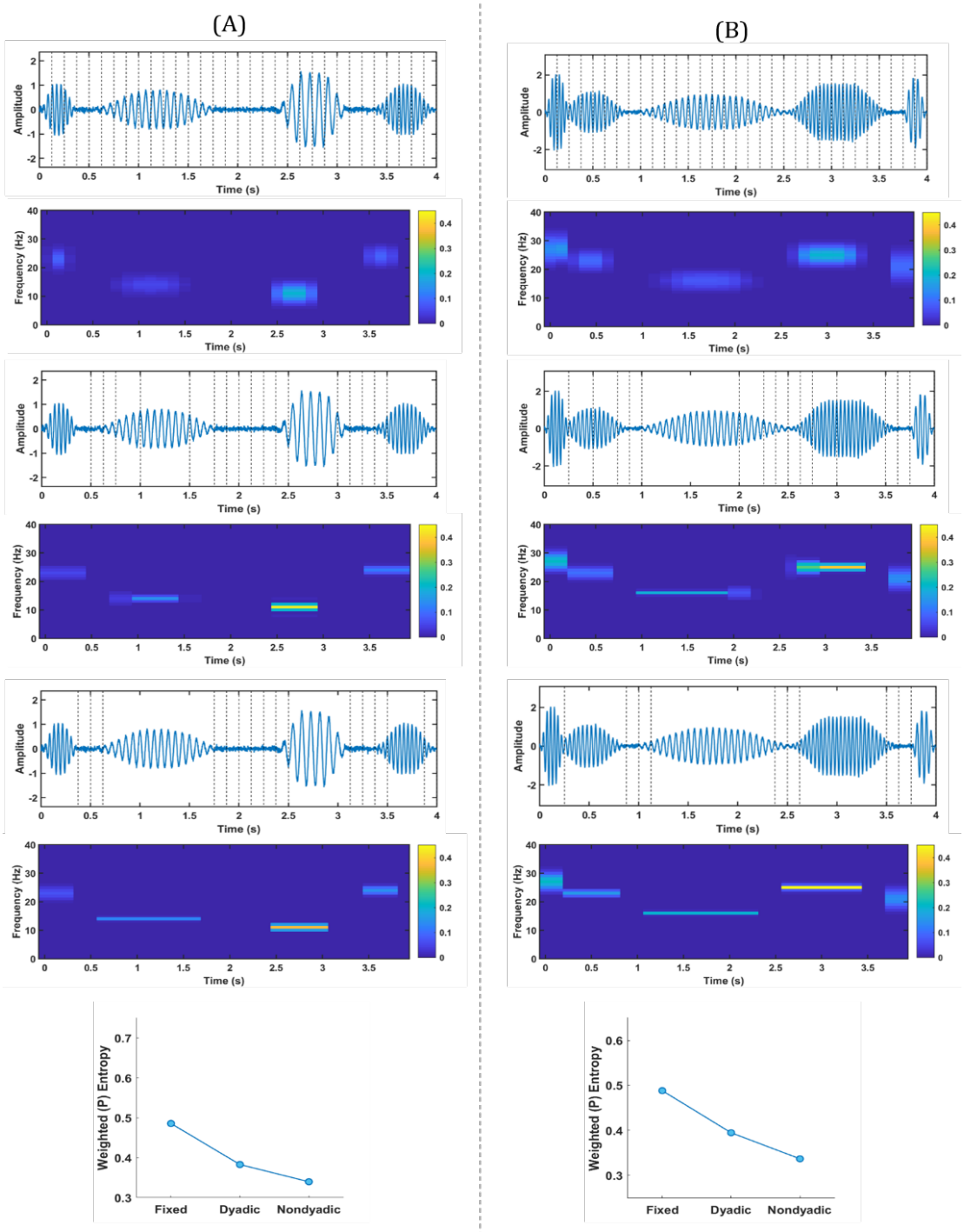

Figure 3. 6: Sides A and B depict two different signals being segmented by the fixed, dyadic and nondyadic algorithms with its corresponding time-frequency map. The weighed (power) entropy average is shown for both signals, for each segmentation algorithm. Weighted entropy average decreased as algorithm accuracy improved.

expected, fixed segmentations had the highest entropy. When dyadic adaptive segmentation is implemented, entropy is not minimized as effectively as the nondyadic version as the segments are constructed at dyadic coordinates.

To quantify the proper function of all three approaches mentioned previously, we created synthetic Gaussian white noise with zero mean and introduced it into all the segmentation algorithms (Figure 3.7). Since there is no structure in the data and samples are independent of each other, we anticipate that the constructed segmentations will not provide any improvement in entropy minimization.

We provided these results in Figure 3.7. We noted that the total entropy values did not change with different segmentation algorithms as we have observed in the previous experiment

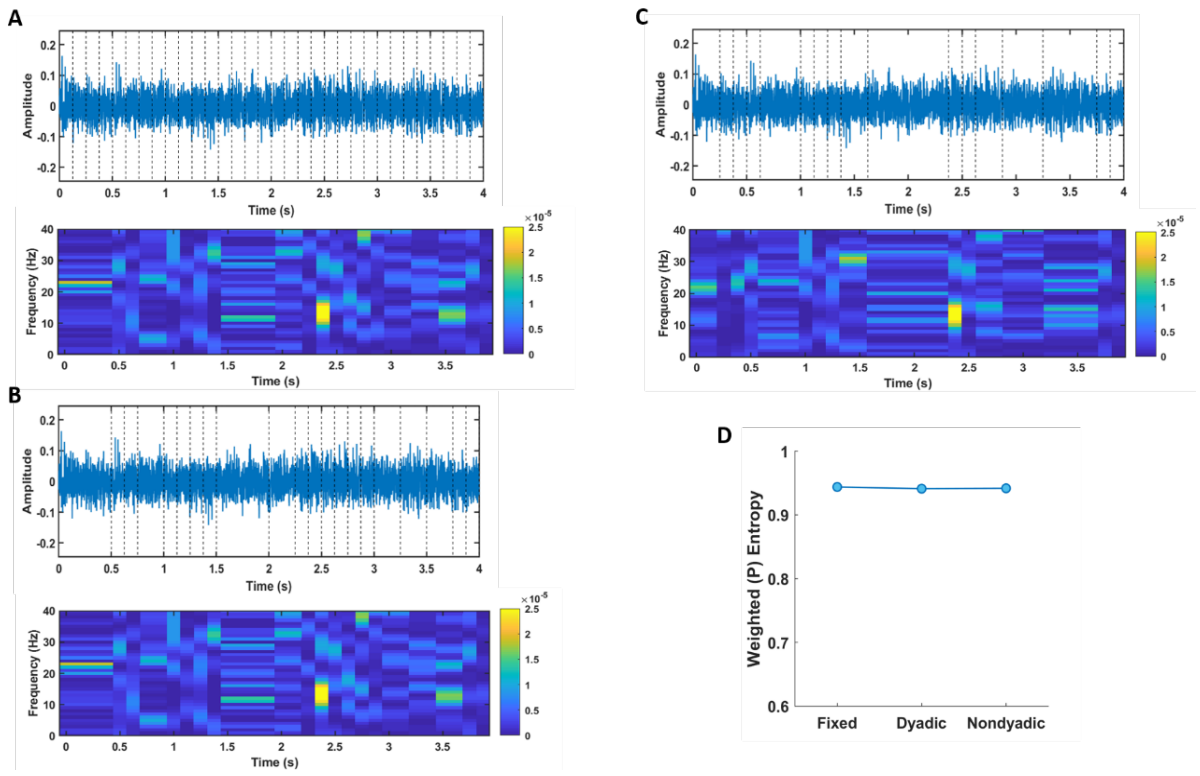

Figure 3. 7: A) Using fixed segmentation on white Gaussian noise. B) Using dyadic segmentation on white Gaussian noise. C) Using nondyadic segmentation on white Gaussian noise. D) Average entropy value of all three segmentation techniques. Weighted average entropy value when using power ratio is also provided.

including localized oscillatory activities. This is an expected result due to the lack of structure or bursts/oscillations in the data.

Based on the experiments, we employed a nondyadic segmentation algorithm on LFP data. We used the minimized entropy between OFF and ON states to predict the symptom improvement of the patients. In the next section, we described our LFP recordings from human subjects with PD and provided our results in detail.

3.3 DATASET AND EXPERIMENTAL PROTOCOLS

In this study, nine patients provided informed consent to be a part of the research study, which was approved by the institutional board of the University of Minnesota and the University of Houston. Participants had to be admitted into the hospital for a 24-Hour DBS electrode recording, after undergoing unilateral DBS electrode implantation of the STN at Fairview Hospital of the University of Minnesota. To reduce discrepancies, the same medication was given to all the patients, and L-DOPA dosages were adjusted to their current medication dosage.

Table 1. Patients Scores and Medication

Pt	Sex	Age	Side	Mean Keyboard Scores (OFF/ON)	Mean Bradykinesia Subscore (OFF/ON)	Mean Total UPDRS Subscore (OFF/ON)	L-Dopa Dose (mg)	Dyskinesia
1	M	70	Left	124.7 / 227.3	9 / 3.7	18 / 5.7	200	None
2	M	43	Left	39.2 / 126.8	13 / 0.3	26.3 / 0.3	500	None
3	M	60	Left	202.83 / 204.6	4.3 / 2.3	7.3 / 3.7	300	None
4	M	68	Left	94.3 / 135	7.3 / 1	12 / 2.8	400	Mild
5	F	62	Right	99.3 / 147.7	12.7 / 2.3	26 / 3.7	200	None
6	**M**	**58**	**Right**	**113.5 / 110.2**	**11.3 / 6**	**17.3 / 9.7**	**150**	**None**
7	M	39	Left	70.2 / 112.8	13.3 / 2	24.7 / 4.7	200	Mild
8	**M**	**54**	**Right**	**84.16 / 100.3**	**11 / 4.3**	**16.5 / 7**	**300**	**None**
9	M	61	Right	124.7 / 219.3	11.7 / 1	17.3 / 3.7	250	Mild

OFF: motor state while not on medication. ON: motor state while on the medication. UPDRS subscores have a maximum value of 32. Bradykinesia has a maximum value of 16. Keyboard scores are the average number of taps for 30 seconds. All scores would be the average of assessments from three different trials. Medication dosages were adjusted to the L-DOPA equivalent. Pt 6 and Pt 8 were given additional medication (50mg) after 30-40 minutes in their first trial because they were not able to achieve the full 'ON' state. Their medication dosages would be the ones given in their two trials.

It is important to note that the two patients (patients 6 and 8) who did not feel improvement with the first dosage of medication administered to them, received a second dose so they could achieve the ON medication state. However, the second dosage of medication did not help with symptom relief, and although their UPDRS scores indicated a slight improvement, their keyboard scores showed minimal to no improvement. Patient scores and prescribed medication dosages are provided in Table 1.

3.3.1 Surgical Procedure and Postoperative LFP Recordings

Using a standard clinical protocol for DBS implantation, Medtronic quadripolar #3389 DBS leads (Medtronic, Minneapolis, MN) were inserted inside the STN of the patients. After three weeks of DBS lead implantation, once admitted into the hospital, the electrodes were externalized, and before Implantable Pulse Generation (IPG) implantation, LFP recordings were collected. The LFPs were recorded using an epilepsy monitoring unit with a wearable amplifier, XLTEK-EMU40, (Natus Medical Inc., Pleasanton, CA) with a 16-bits analog-to-digital converter with an antialiasing filter at 400 Hz at a sampling frequency of 1024 Hz. The

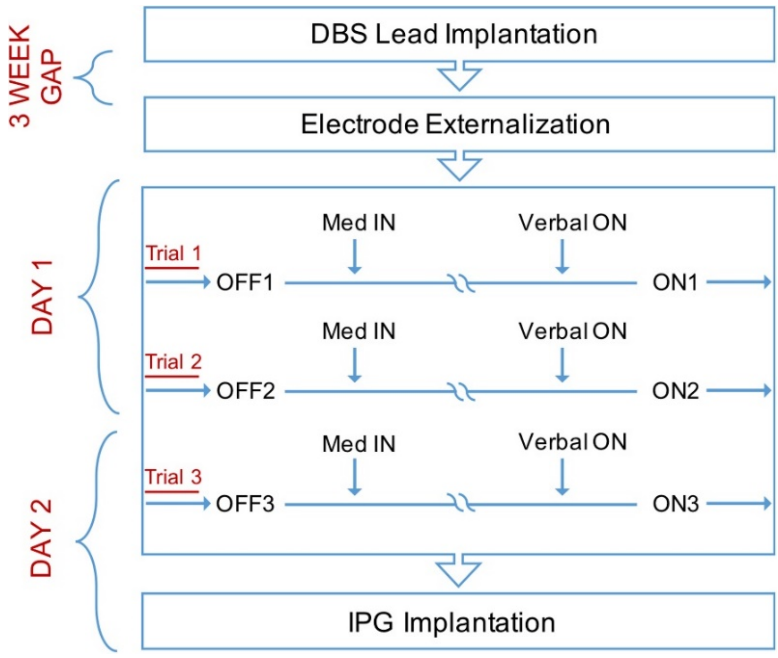

Figure 3. 8: Recording Timeline. The 24-Hour LFP recordings of patients began 3 weeks after DBS lead implantation. The study consisted of 3 trials period. Reproduced from Ozturk et al., [2019].

LFP recordings were collected from all four monopolar DBS lead contacts and were high-pass filtered at 0.1 Hz to remove any DC-offset.

At least 12 hours after their last medicated dosage, 30 minutes recording undertook place for each patient during their first OFF state and was used as a baseline recording. Proceeding the previous recording, L-DOPA was administered to the patients (med in), and they were directed to announce once they felt their medication set in (verbal on). Subsequently, once symptoms began to resurface, the patient announced their medication had worn off, therefore completing one trial. In total, this study comprised of three trials, and it is accurately summarized in Figure 3.8.

3.3.2 Patient Assessments and Completed Task

The UPDRS III (motor section) was used in each state to quantify the patient's clinical impairment before and after medication. The subsections of particular interest were hand and foot tremor, upper and lower extremity rigidity, and finger tapping, hand open and close, lastly, hand supination/pronation. Also, patients were instructed to complete a keyboard task during each state. For the keyboard task, the patient had to alternately press two different keys for 30s following a 10s resting period. The task was completed twice in each state, and all press errors were taken into count during the timing period. Each patient was evaluated 30 minutes before being administered their medication, and 30 minutes after announcing their medication had taken effect. Furthermore, patients were also instructed to rest for a minimum of 120s in each OFF and ON state.

3.4 REST DATA PREPROCESSING

3.4.1 Bipolar Derivations

Resting data was recorded continuously for a minimum of 120s. It was then inspected with an in-house software, CNELab [Jiang et al., 2017]. LFPs were recorded using monopolar contacts LFP 0, LFP 1, LFP 2, LFP3, and LFP 3. Subsequently, a montage was used to derive the bipolar derivations of the monopolar contacts by subtracting adjacent channels [Ozturk et al., 2019]. The benefits of using bipolar derivation would be that spatial resolution increases and the correlative activity of the signal is removed [Meloni et al., 2015]; this allows a clear visualization of beta bursts during the OFF (Figure 3.11 A) and ON (Figure 3.11 B) medication state. Apparent suppression of beta bursts is visualized in the ON state, which is also confirmed by the patient's power spectra (Figure 3.12 A).

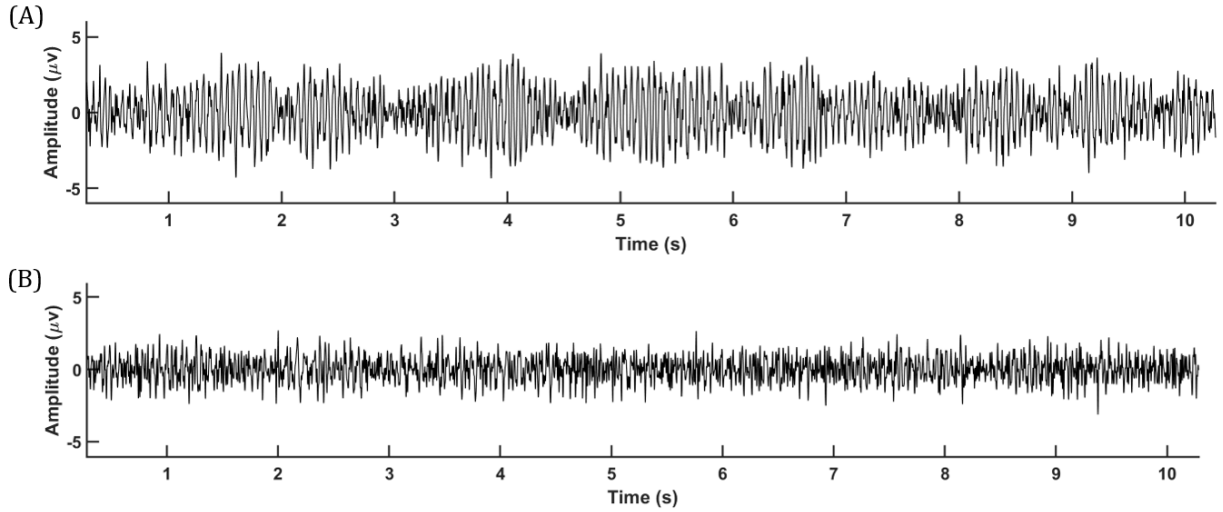

Figure 3. 9: A) LFP recording of OFF medication state, beta bursts are visible. B) LFP recording of ON medication state, beta bursts have been suppressed by medication.

3.4.2 Power Spectra

The power spectra of bipolar derivations for each patient in different states were computed using the welch periodogram method. A Hanning window length of 1,024 samples with a 50% overlap and a frequency resolution of 1 Hz was used to calculate the power spectrum of each OFF and ON state and grand average (Figure 3.10). Based on these results, the bipolar derivation with the largest beta band power in the OFF-medication state was chosen for each patient (Table 2).

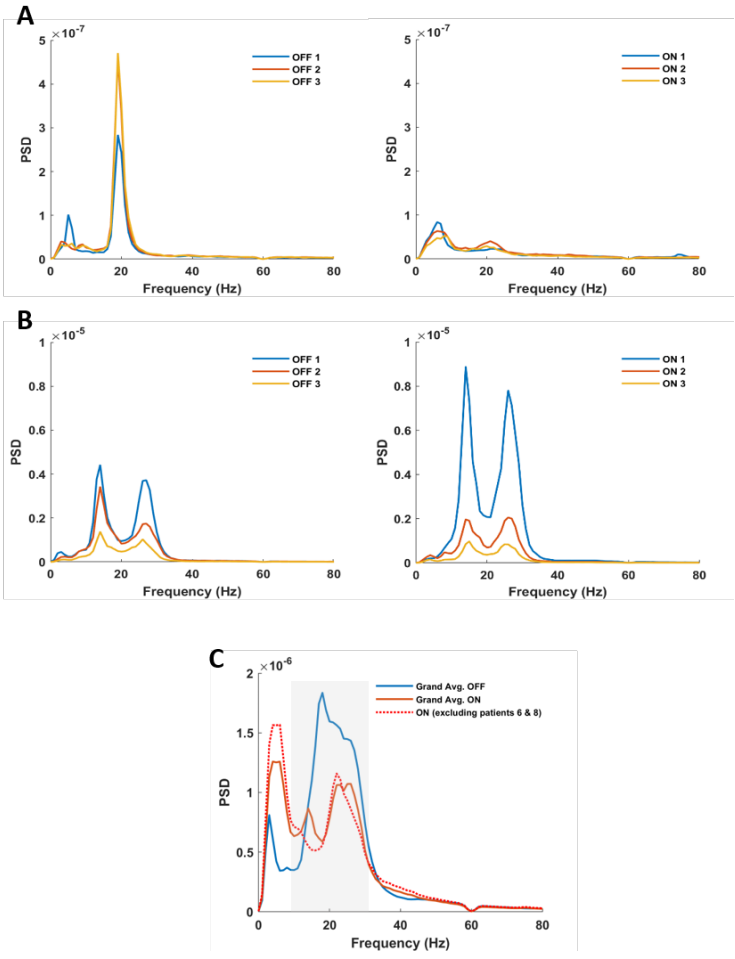

Figure 3. 10: The images on the left represent the OFF state, and those on the right represent the ON state. A) Power spectral density of Pt 2, who improved after the administration of L-DOPA. B) Power spectral density of Pt 6 who did not improve after the administration L-DOPA. C) Blue: PSD grand average of OFF state, Red: PSD grand average of ON state, Dotted-Red: PSD grand average of ON state when excluding patients 6 and 8. The shaded area highlights the beta range used (13-30Hz).

Table 2. Patient's Optimal Bipolar Derivation

Patient	Optimal Bipolar Derivation
1	E02
2	E01
3	E12
4	E01
5	E12
6	E01
7	E12
8	E12
9	E12

The optimal contact pair chosen for each patient are shown. Optimal contacts were chosen based on the highest beta power that was present during the OFF medication state for each patient.

3.4.3 Filtering

Before completing any further analysis of the signal, the LFP data were high passed filtered above 8Hz with a 385 tap FIR filter (designed using Blackman window). Zero-phase filtering was then applied to have zero-phase distortion, thus preserving the original characteristics of the signal. Subsequently, a 60Hz Butterworth-IIR notch filter of 2^{nd} order was used to remove powerline artifacts, and zero-phase filtering was applied once again.

CHAPTER IV

RESULTS

4.1 PATIENT IMPROVEMENT

Figure 4.1 depicts the improvement that is seen in the patients with their mUPDRS, keyboard, and bradykinesia scores. In the three scores we observed a significant difference between the two states, confirming patient improvement and efficacy of the medication.

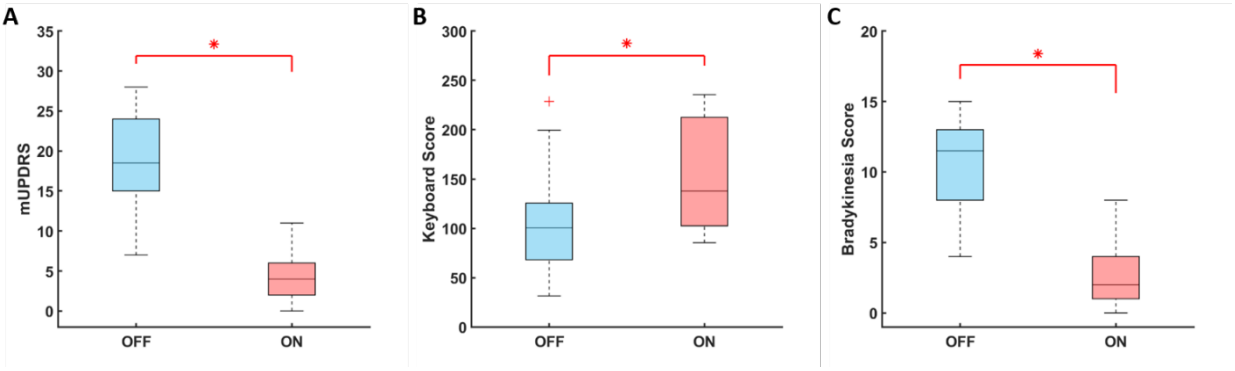

Figure 4. 1: Difference in scores during OFF and ON states, the Wilcoxon rank-sum test was used in all. A) mUPDRS, $p<0.001$. Mean-OFF: 18.5 and Mean-ON: 4.3. B) Keyboard task scores, $p=0.002$. Mean-OFF: 105.9 and Mean-ON: 151.3. C) Bradykinesia sub-scores, items: 23-26, $p<0.001$. Mean-OFF: 10.5 and Mean-ON: 2.4

4.2 ADAPTIVE BETA BURSTS SEGMENTATION

Once the resting data was preprocessed, it was ready to be introduced in the adaptive segmentation algorithm. The nondyadic adaptive algorithm was able to segment beta bursts (Figure 4.2 and 4.3) from LFP recordings during the OFF-medication state efficiently, and the time-frequency map confirmed it. Longer segments in the OFF-medication state, have a higher beta power, thus smaller segments had little to no beta power present. Figure 4.2 represents patient 2 during different OFF and ON medication states. While Figure 4.3 depicts patient 1 during two different OFF and ON medication states. During the ON medication state, segments with a higher beta power were not as present, and the data was segmented into smaller segments than before, as presented in the following segments.

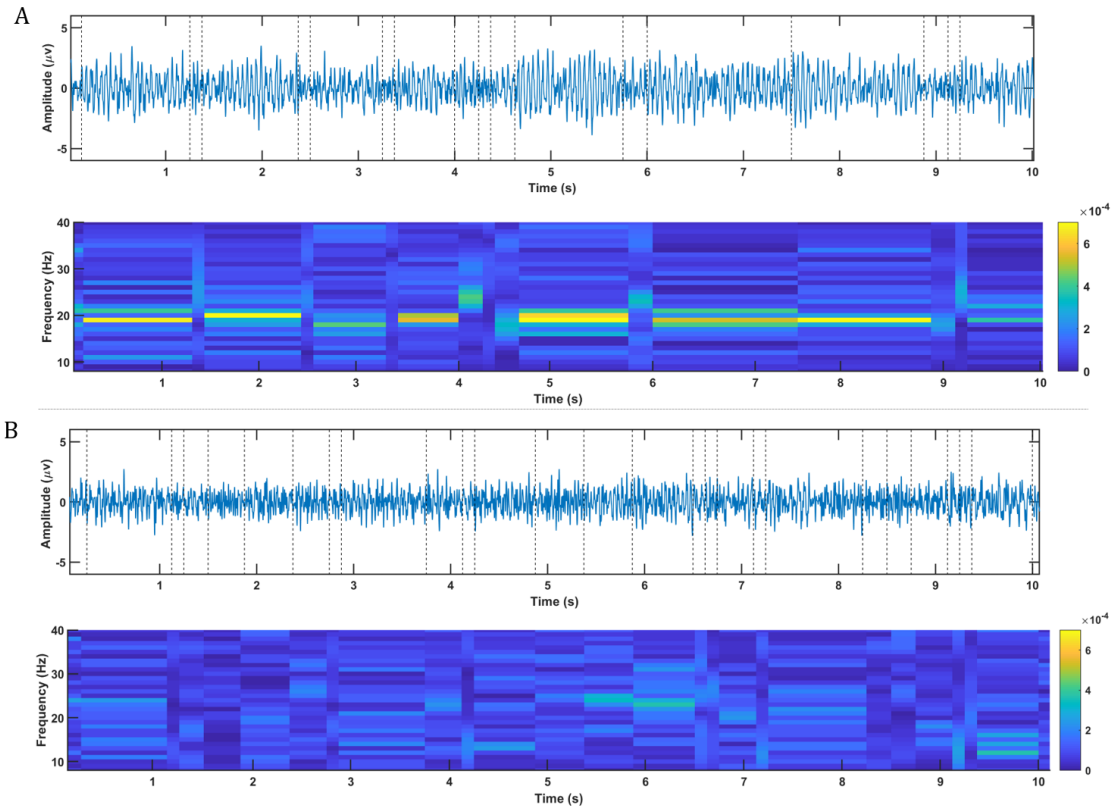

Figure 4. 4: A) Nondyadic segmented LFP recording of Patient 2 during the first OFF trial, with its according time-frequency map. B) Nondyadic segmented Patient 2 LFP recording during first ON trial, with its according time-frequency map.

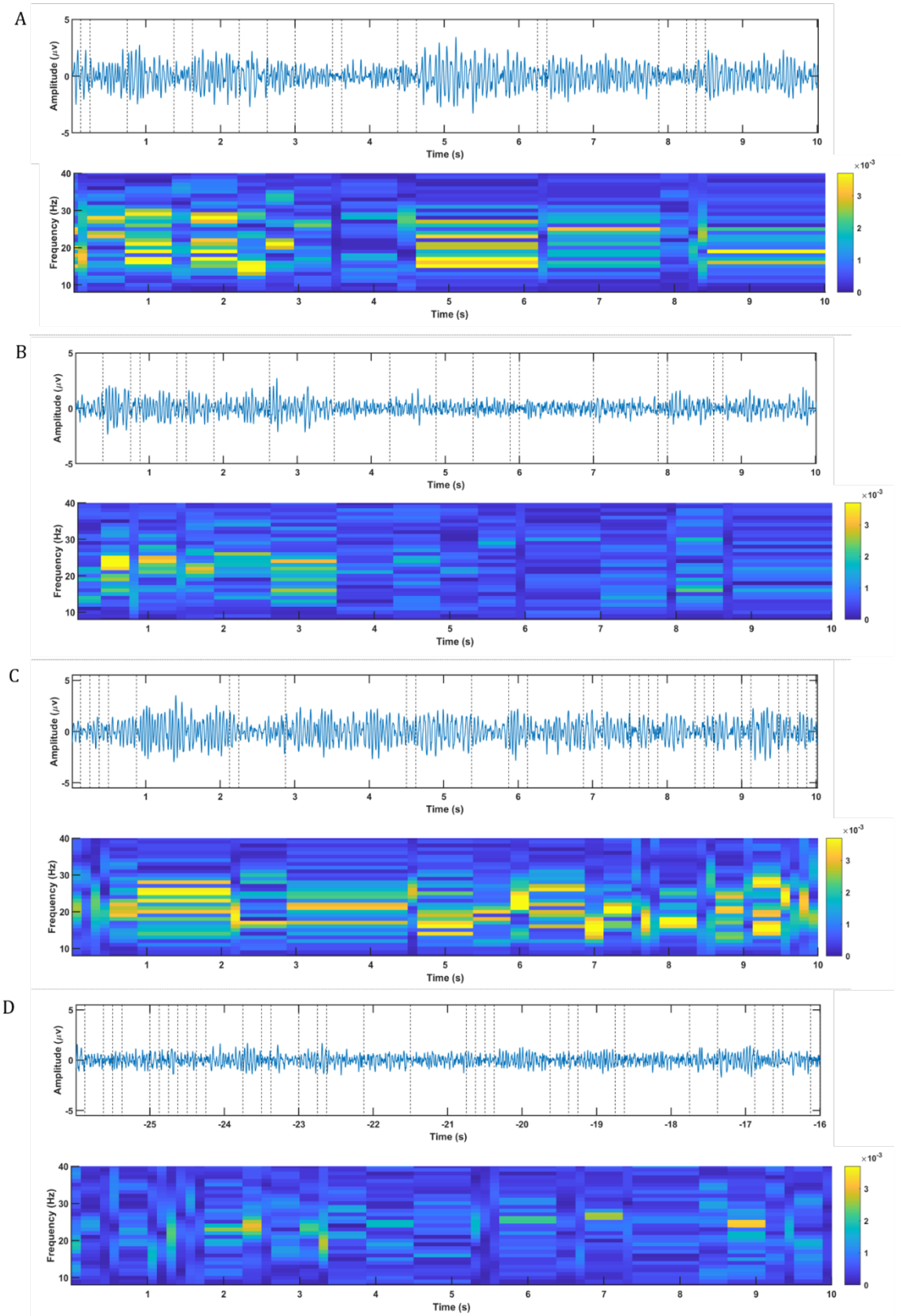

Figure 4. 7: A & B) Nondyadic segmented LFP recording of Patient 1 during OFF1(A) and ON1 (B) trial, with its according time-frequency map. C & D) Nondyadic segmented LFP recording of Patient 1 during OFF3 (C) and ON3 (D) trial, with its according time-frequency map.

4.2.1 Distribution of Constructed Segments

We binned segments in the following way, 0.125, 0.250, 0.375, 0.50, 0.625-0.875, and ≥ 1 s (Figure 4.4), and found that larger bursts were present during the OFF-medication state. Since medication results in the reduction of beta power in the ON state, ON state segments were not expected to include structured large-amplitude beta oscillations of long duration. For this reason, considering the background noise and lack of beta bursts, the algorithm segmented the ON state into the shortest segment possible to aid in the minimization of entropy.

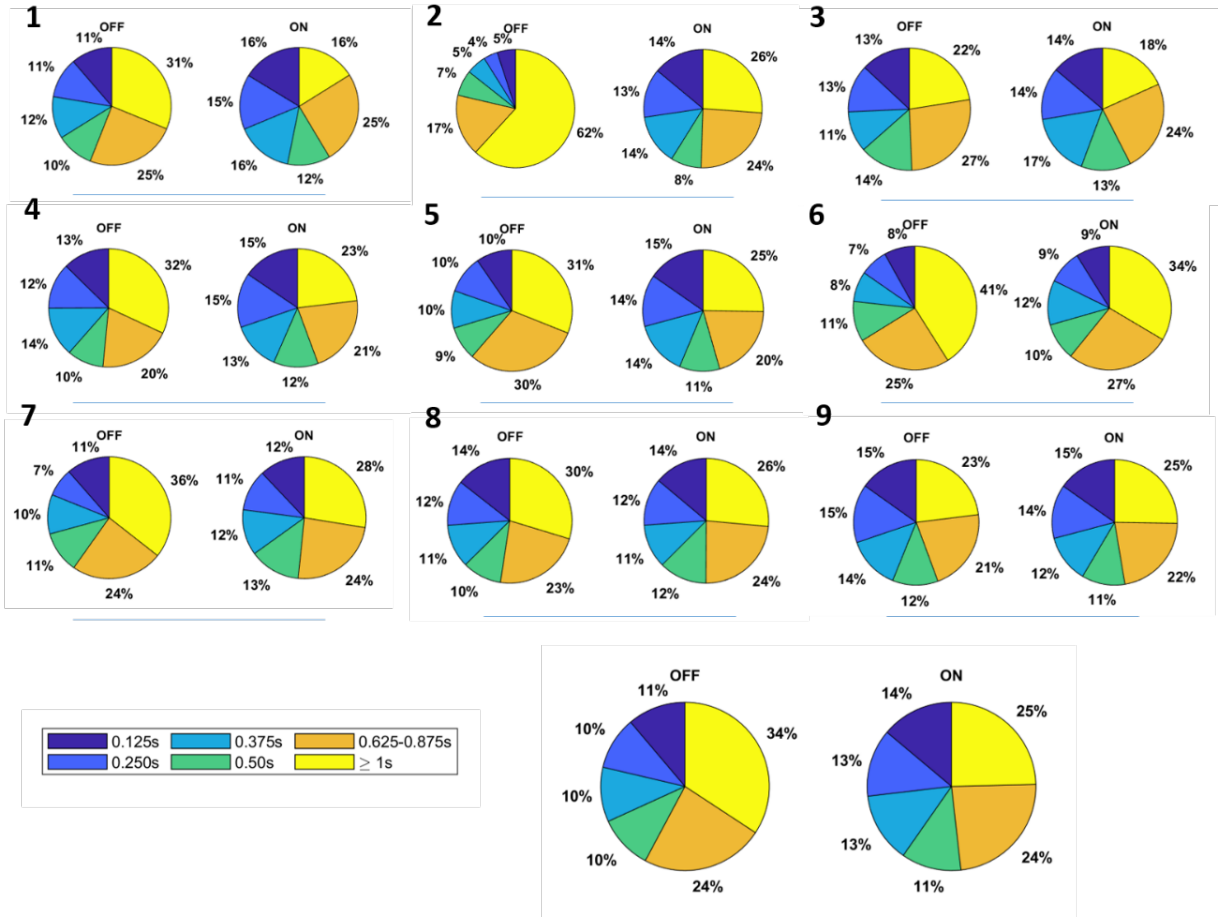

Figure 4. 10: The pie charts represent how much of the data is made up by the segments of that specific length for the different OFF and ON states. The bottom two pie charts represent the average across of all the patients for their OFF and ON state.

Hence, the number of smaller segments which make up the data in the ON state will increase. Overall, we noted a significantly ($p = 0.01$) larger amount of short (=0.125s) segments in the ON states compared to the OFF states. They accounted for 14% of the ON state data and 11% in the OFF state data. On the contrary, we observed a significantly ($p < 0.05$) larger number of ≥1s segments in the OFF states compared to the ON states (Figure 4.5). These long segments accounted for 25% of the ON state data and 34% of the OFF state data. The verification of the increase in smaller segments and a decrease in larger segments during the patients' ON-medication state helps to partially explain patient improvement.

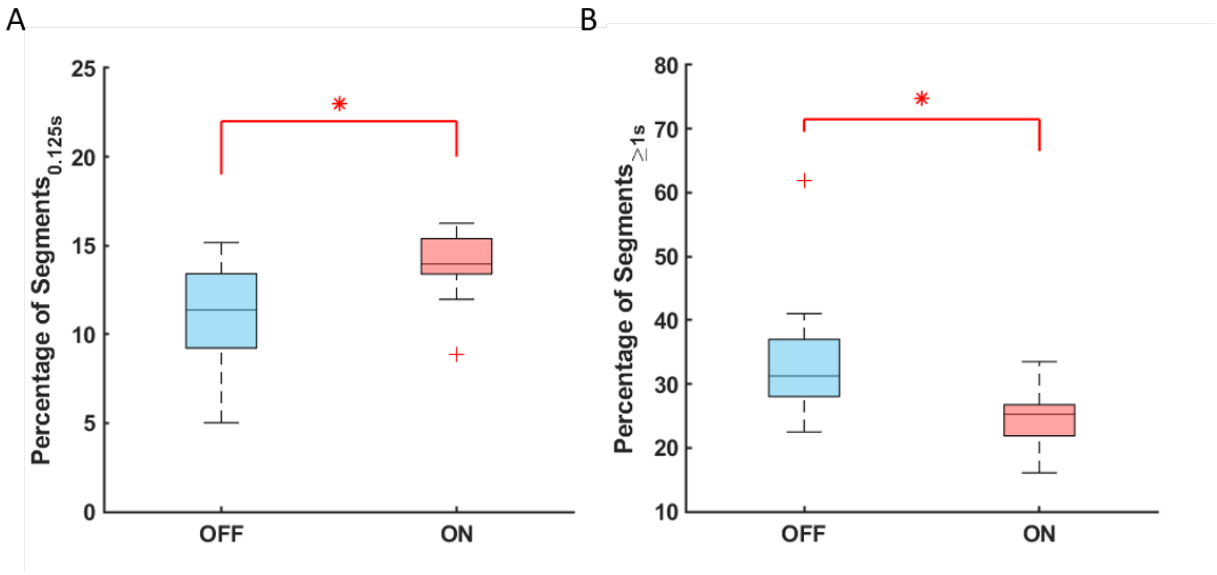

Figure 4. 13: Difference in segments during OFF and ON states, the Wilcoxon signed-rank test was used for both. A)The Boxplots show the difference in the smallest segment (0.125s) between OFF and ON states, all patients included (p=0.01). B) The Boxplots show the difference in segments ≥ 1s between OFF and ON states, all patients included (p<0.05).

4.3 ENTROPY OF SEGMENTS

After the construction of the segments, their entropy was computed. We visualized the mean entropy of each segment size for each patient during their OFF and ON states. We then plotted four curves for each patient representing the three OFF-ON medication trials and an

overall average of all trials (Fig. 4.6). For those patients who improved based on their UPDRS and keyboard scores, we observed that they had a clear separation of their entropy curves (Figure 4.6A). However, our results show that for those two patients (patients 6 and 8) who did not improve, their entropy curves did not exhibit separation (Figure 4.6B). This disconnect of the entropy curves between the OFF and ON medication states is caused by the number of beta bursts that are captured in each state. Therefore, as segment size increases, mean entropy decreases in the OFF state, which is caused by longer beta oscillations that were captured by the adaptive segmentation algorithm.

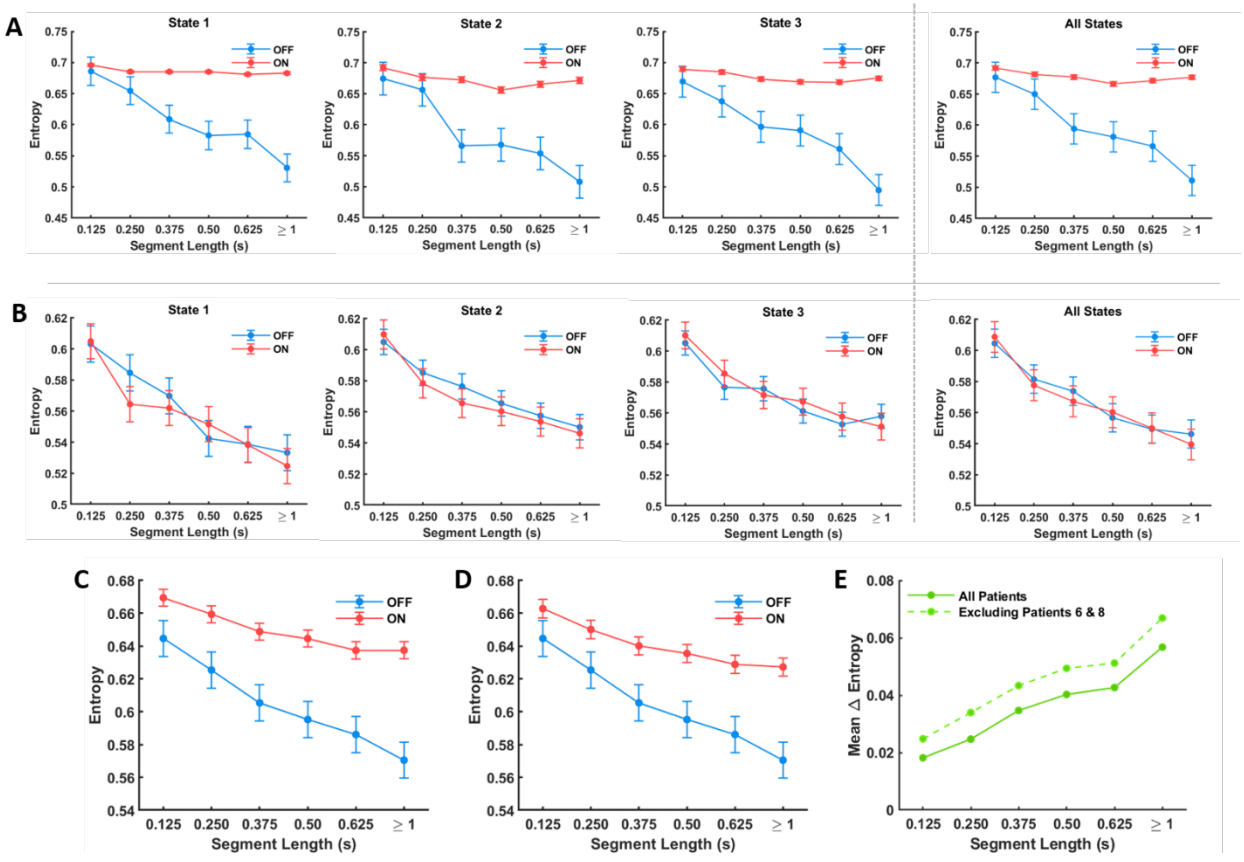

Figure 4. 16: The 0.625s index on x-axis represents segments between 0.625s and 0.875s. A) Entropy curves of Patient 2 for separate states and overall average included. B) Entropy curves of Patient 6 for all separate states and overall average. C) Overall average when excluding the ON trials of patients 6 and 8. D) Overall average when including the ON trials of patients 6 and 8. E) Entropy difference for different segment lengths, when using all patients (solid line) and excluding patients 6 and 8 (dashed line) from ON state.

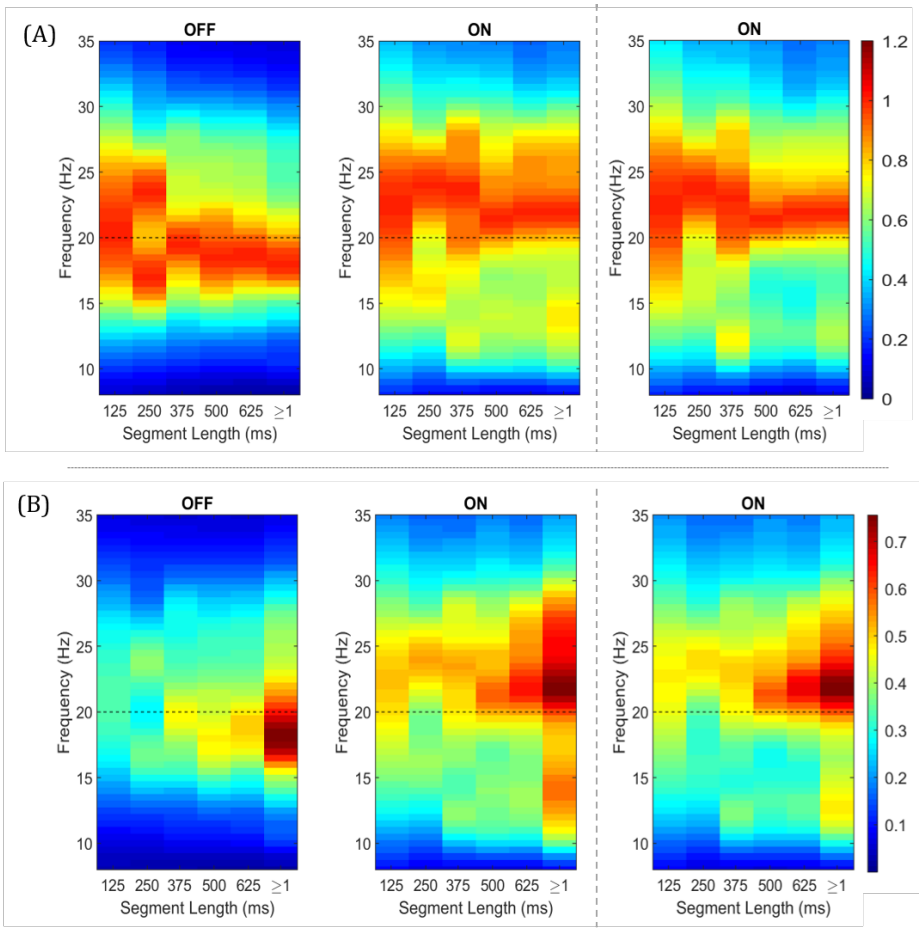

Figure 4. 19: In the first two columns, beta spectrum of the grand average of all patients for OFF and ON trials is presented, while the ON trials after the dotted gray line excludes the two patients (6 & 8) who did not improve. The 0.625s index on x-axis represents segments between 0.625s and 0.875s. (A) Normalization of the power spectrum in each segment to its maximum power. (B) Power of all segments was normalized to the maximum beta power across all segments.

On the other hand, during the ON medication state, longer beta bursts are not recurrent, while shorter segments are thus increasing the mean entropy for each segment bin.

We observed that as segment size increases, the difference between the OFF and ON entropy curves enlarges; this led us to compute two grand averages to determine how the patients who did not improve would affect the average across all patients. The first average excluded patients 6 and 8 from the ON state (Fig 4.6C), while the second average includes all subjects

(Fig. 4.6D). An increase in the entropy for the ON state curve is seen when removing patients 6 and 8. This difference emphasizes the influence that patients 6 and 8 had on the increase/decrease of the mean ON state segment entropy, respectively. Figure 4.6E depicts the difference between the mean entropy for each time window. As we expected, the difference in entropy increases when excluding the two patients who did not improve from the ON state.

When we normalized the power spectrum in each segment to its maximum power and averaged it over subjects (Figure 4.7A), it helped confirm the presence of beta in each segment bin. During the OFF-medication state, low-beta (13-22Hz) power was present in all segments, and it then shifted to high-beta (23-30Hz) power during the ON-medication state, which shows the suppression of low beta by L-DOPA. When we excluded patients 6 and 8 from the ON state, the presence of low-beta power is diminished. Moreover, when we normalized the power spectrum in each segment to the maximum power across all segments and averaged it over subjects, beta band power increased with respect to segment length (Figure 4.7B).

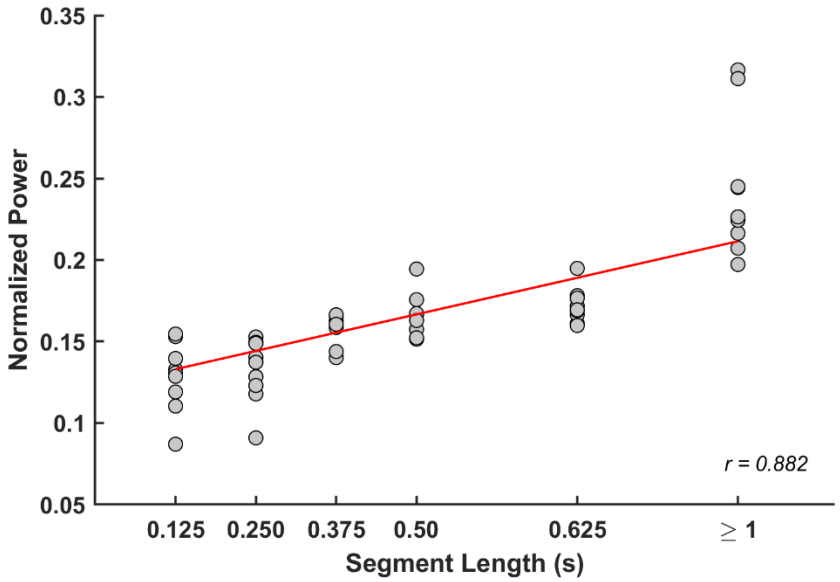

Figure 4. 22: Normalized OFF state beta band power across all segments was positively correlated to increasing segment length (r=0.882, p<0.05). The 0.625s index on x-axis represents segments between 0.625s and 0.875s.

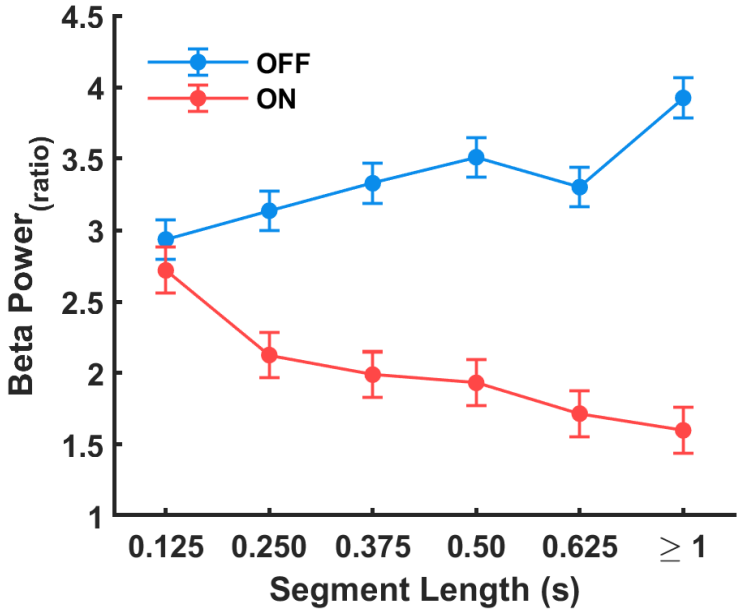

Figure 4. 25: Overall average of the change in beta-power ratio with respect to segment length for OFF and ON state. The 0.625s index on the x-axis represents segments between 0.625s and 0.875s.

Once again, by removing the two patients who did not improve, we can visualize the peak frequency shifting from low-beta to high-beta when transitioning from OFF to ON state. When we normalized OFF state beta band power across all segments for each patient, we were able to determine how much of the beta power lied within each segment bin. Therefore, if the normalized power from each segment bin was summed up for each patient, it would equal to 1. This normalized beta power was positively correlated ($r = 0.882, P < 0.05$) with increasing segment length (Figure 4.8). Meaning that normalized beta band power had little to no presence in smaller segments, but as segment length increased the presence of this normalized power became more pronounced. Affirming the previous findings of the entropy curves, as beta power increases, entropy is minimized. Consequently, the drop seen in the entropy curves at $\geq 1s$, was due to beta power increasing for segments $\geq 1s$.

We also calculated the beta-power ratio

$$Power_{ratio} = \frac{\beta_{low}}{\beta_{high}}, \tag{4.1}$$

where β_{low} represents the low-beta frequency range (13-22Hz), and β_{high} represents the high-beta frequency range (23-30Hz). We used the beta-power ratio to determine the presence of low-beta in all segments, which has been related to the pathological part of PD. During the OFF state, low-beta power increased gradually as segment size increased, and as expected, low-beta power decreases in the ON state with respect to segment size (Figure 4.9).

4.4 CLINICAL CORRELATION

We correlated the difference in entropy for each segment bin with the difference in mUPDRS scores and found the correlation coefficient for each segment length to plot the correlation curve (Figure 4.10A) The correlation coefficient steadily increased when we correlated the difference in entropy for specific segment lengths with difference mUPDRS scores. When we weighted segments with their beta power ratio, the correlation coefficient curve increased steadily as well (Figure 4.10B). We obtained a poor correlation when establishing the correlation between the smallest segment (0.125s) and Δ mUPDRS scores ($r = -0.165, P = 0.41$), suggesting that smaller segments may not be the leading cause of clinical impairment (Figure 4.10C). The suppression of larger and longer beta oscillations is caused by L-DOPA, resulting in a sizeable difference in entropy. Therefore, longer segments ($\geq$ 1s) had a strong positive correlation ($r = -0.749, P < 0.001$) to clinical improvement (Figure 4.10D). Additionally, when we included all segments by weighting them with their respective beta-power ratio, correlation increased ($r = -0.825, P < 0.001$) (Figure 4.10E).

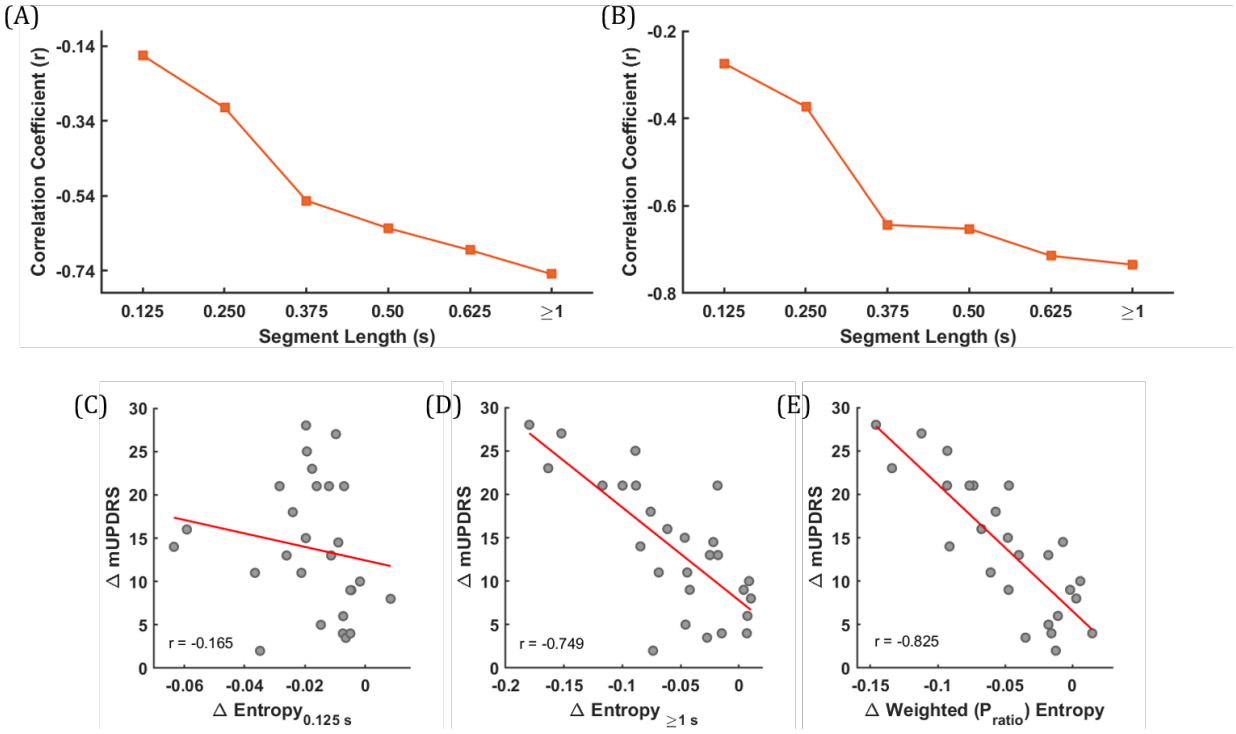

Figure 4. 28: A) Correlation coefficient for difference in mUPDRS vs difference in entropy was plotted for each segment bin and a curve was obtained. B) Correlation coefficient curve for weighted segments of difference in mUPDRS. B) Correlation of difference in mUPDRS with the difference in entropy from segments of 0.125s. C) Correlation of difference in mUPDRS with the difference in entropy from segments of 1s and greater. D) Correlation of difference the in mUPDRS with difference in weighted entropy (using power ratio) for all segments.

We calculated the percent change in the keyboard scores as

$$Improvement\ (\%) = \frac{[ON\ -OFF]}{OFF} \times 100, \tag{4.2}$$

where *ON* represents the score from the ON state, and *OFF* represents the score from the OFF state. We then correlated the difference in entropy for each segment bin with keyboard improvement and a similar trend to that of the mUPDRS scores was noted. We plotted each correlation coefficient to obtain a curve, and for a second time, we observed that an increase in segment size resulted in the rise of correlation for each segment length (Figure 4.11A). However, when weighing the entropy of these segments with its beta power ratio, the curve fluctuated for

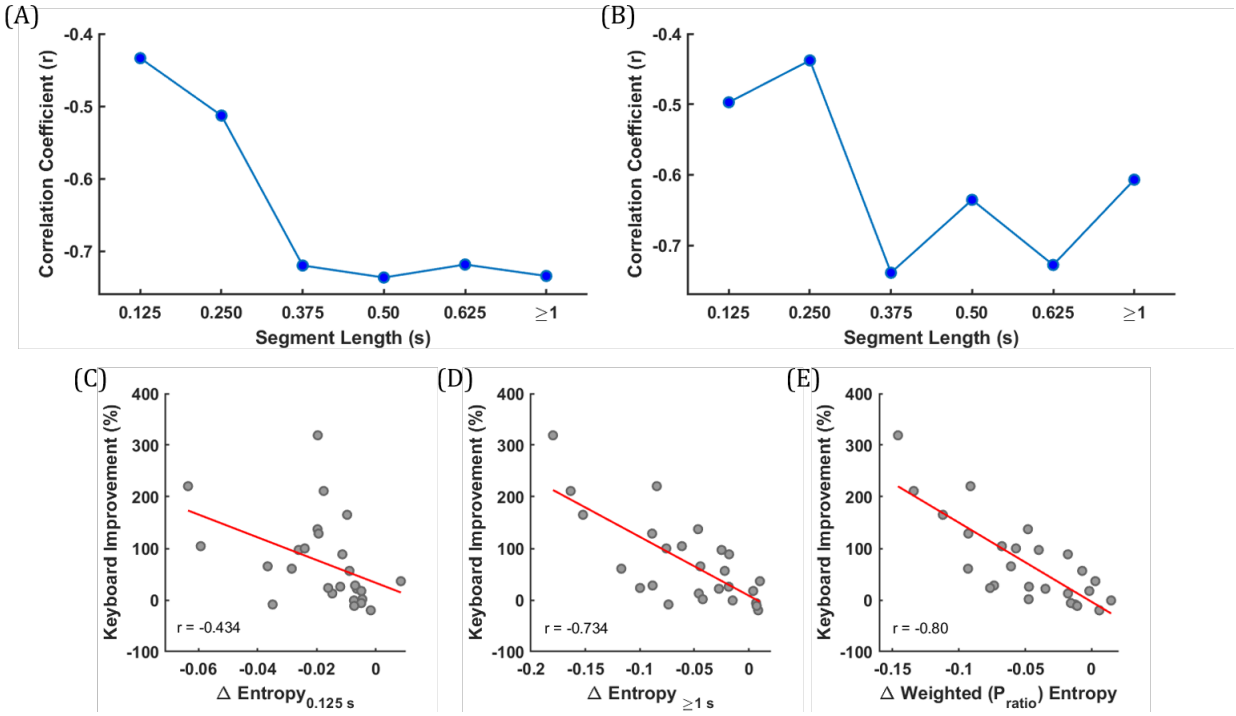

Figure 4. 31: A) Correlation coefficient for keyboard improvement (%) vs difference in entropy was plotted for each segment bin and a curve was obtained. B) Correlation coefficient curve for weighted segments of keyboard improvement. C) Correlation of keyboard improvement (%) with the difference in entropy from segments of 0.125s. D) Correlation of keyboard improvement (%) with the difference in entropy from segments of 1s and greater. E) Correlation of keyboard improvement (%) with the difference in weighted entropy (using beta power ratio) for all segments.

some segment lengths (Figure 4.11B). This signified that some patient's low-beta bursts may lie within a specific beta-range resulting in the decreased correlation. The difference in entropy for the $0.125s$ segments had a weak correlation ($r = -0.434\,, P < 0.05$) with keyboard improvement, once again indicating that the presence of smaller segments may not impact a patient negatively (Figure 4.11C). When we correlated the difference in entropy of segments $\geq 1s$ ($r = -0.734, P < 0.001$) with clinal improvement there was a strong correlation (Figure 4.11D). Correlation improved ($r = -0.80, P < 0.001$) even further when we used all of the segments to correlate them to the clinical improvement by weighting their entropy with the beta power ratio, suggesting that the low-beta bursts can be related to the clinical impairment the patient experiences (Figure 4.11E).

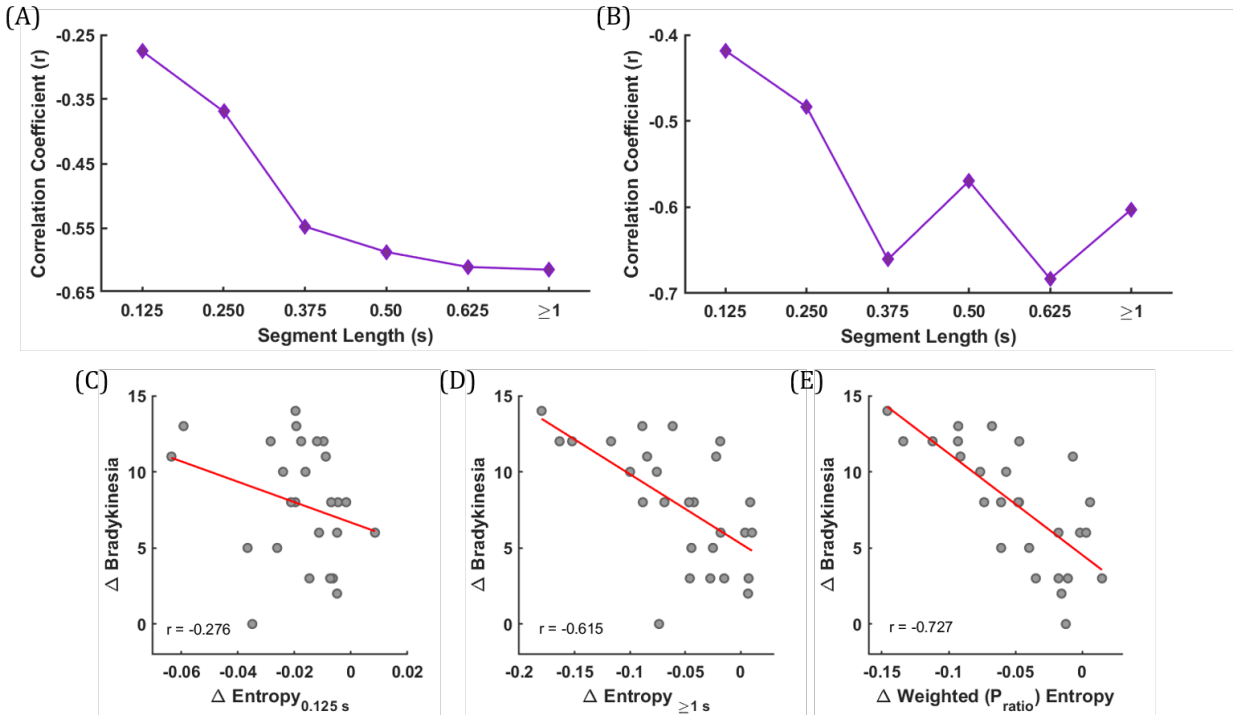

Figure 4. 34: A) Correlation coefficient for difference in bradykinesia score vs difference in entropy was plotted for each segment bin and a curve was obtained. C) Correlation of difference in bradykinesia score with the difference in entropy from segments of 0.125s. D) Correlation of difference in bradykinesia score with the difference in entropy from segments of 1s and greater. E) Correlation difference in bradykinesia score with the difference in weighted entropy (using beta power ratio) for all segments.

Additionally, we correlated the difference in entropy with the difference in bradykinesia scores and plotted the correlation coefficient for each segment bin (Figure 4.12A). When we weighted the segments with its beta power ratio, the curve fluctuated as it did for the weighted keyboard improvement curve (Figure 4.12B). Moreover, smaller segments exhibited a weak correlation ($r = -0.276, P = 0.2$) to the difference in bradykinesia scores (Figure 4.12C). However, longer segments ($\geq$ 1s) did have a strong correlation ($r = -0.615, P < 0.001$) with difference in bradykinesia scores (Figure 4.12 C). Furthermore, by weighing all the segments with their power ratio, we found that they were highly correlated to difference in bradykinesia scores ($r = -0.721, P < 0.001$) (Figure 4.12D).

Table 3. Correlation Coefficient of Different Segmentation Algorithms

Segmentation Algorithm	ΔmUPDRS	Keyboard Improvement (%)	ΔBradykinesia
Fixed Segmentation	-0.79	-0.726	-0.72
Best Basis/Dyadic	-0.788	-0.835	-0.71
Nondyadic Segmentation	-0.825	-0.80	-0.727

All three segmentation algorithms were used to segment the LFP data. The entropy of the segments were weighted with their beta power ratio and correlated to Δ mUPDRS scores, keyboard improvement (%), and Δ Bradykinesia scores.

We also used fixed segmentation, and Best basis/Dyadic segmentation to segment the LFP data. We then weighted the entropy of the corresponding segments from each segmentation algorithm with the beta-power ration and correlated the weighted segments with keyboard improvement (%), Δ mUPDRS scores, and Δ Bradykinesia scores. Fixed segmentations were correlated with keyboard improvement ($r=-0.726$, $p<0.001$), difference in mUPDRS scores ($r=-0.79$, $p<0.001$), and difference in bradykinesia scores ($r=-0.72$, $p<0.001$). Best Basis/Dyadic segmentations were also correlated with keyboard improvement ($r=-0.835$, $p<0.001$), difference in mUPDRS scores ($r=-0.788$, $p<0.001$), and difference in bradykinesia scores ($r=-0.71$, $p<0.001$). Additionally, as mentioned previously nondyadic weighted segments were also correlated to keyboard improvement ($r=-0.80$, $p<0.001$), difference in mUPDRS scores ($r=-0.815$, $p<0.001$), and difference in bradykinesia scores ($r=-0.27$, $p<0.001$). Overall, the segments obtained from nondyadic segmentation gave the best correlation because of the way beta bursts were captured and segmented.

We then correlated the entire beta band power, and low-beta power to keyboard and UPDRS scores (Figure 4.13A). We found a significant correlation when the full beta band (13-30 Hz) ratio (ON/OFF) was correlated to keyboard improvement (%) ($r = -0.651, P < 0.001$) and mUPDRS scores ($r = -0.599,\ P < 0.001$). These correlation values were similar when solely using low-beta band power (Figure 4.13B). For keyboard improvement, the correlation was -0.634 ($P < 0.001$) whereas, mUPDRS correlation to low-beta band power was -0.677 ($P < 0.001$).

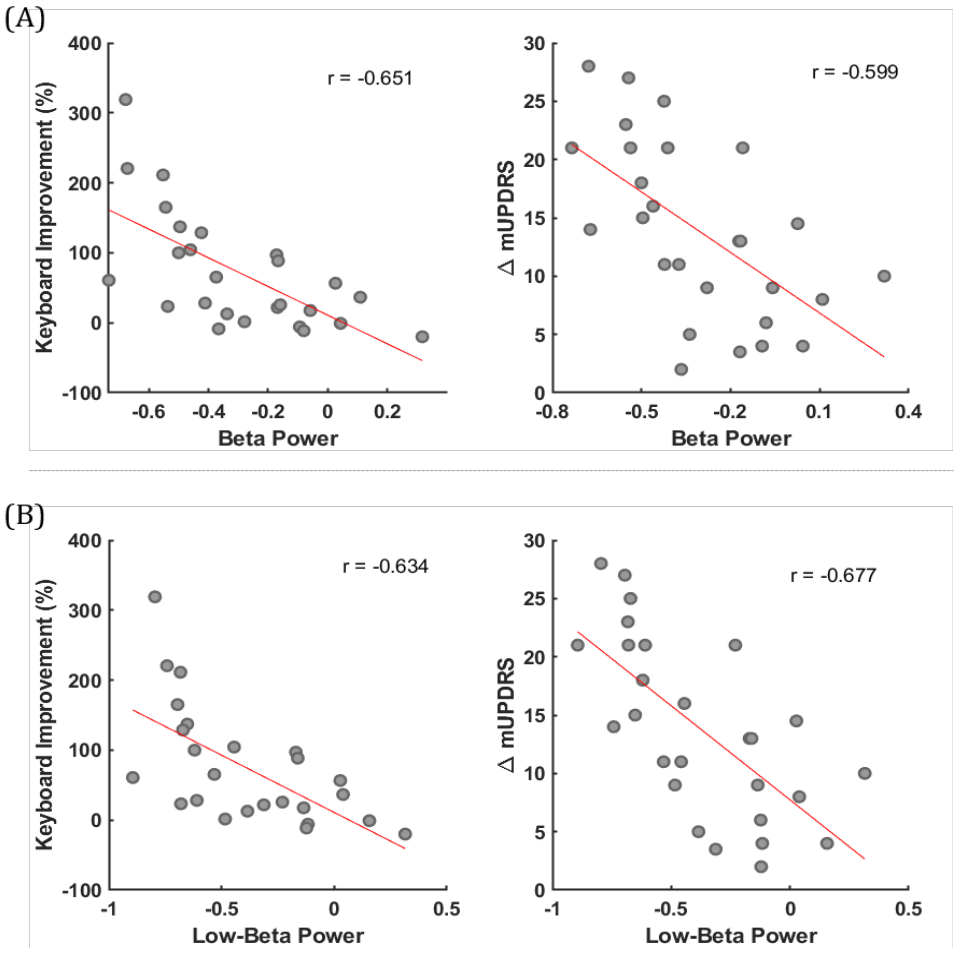

Figure 4. 37 : A) Full beta-band (13-30Hz) power log-ratio (ON/OFF) correlation to keyboard improvement (r = -0.651, P<0.001) and mUPDRS (r = -0.599, P<0.001). B) Low-beta band power (13-22Hz) log-ratio correlation to keyboard improvement (r = -0.634, P<0.001) and mUPDRS.(r = -0.677, P<0.001)

The entropy sum that we used was based on the entropy sum of all segments during the first OFF state for each patient, also referred to as the total entropy. We then correlated total entropy to the total UPDRS scores and the individual subscores (Figure 4.14). Total UPDRS (r=-0.573, p=0.11), rigidity (r=-0.69, p=0.04), and bradykinesia plus rigidity (r=-0.617, p=0.08) were correlated to entropy gain. While, bradykinesia (r=-0.479, p=0.2), and tremor (r=-0.202, p=0.6) had little to no correlation to entropy gain. However, although these correlations were not significant, it still gives a brief understanding of how total entropy is related to the first OFF medication state of the patients. The correlation might improve and become more significant if we had additional patients.

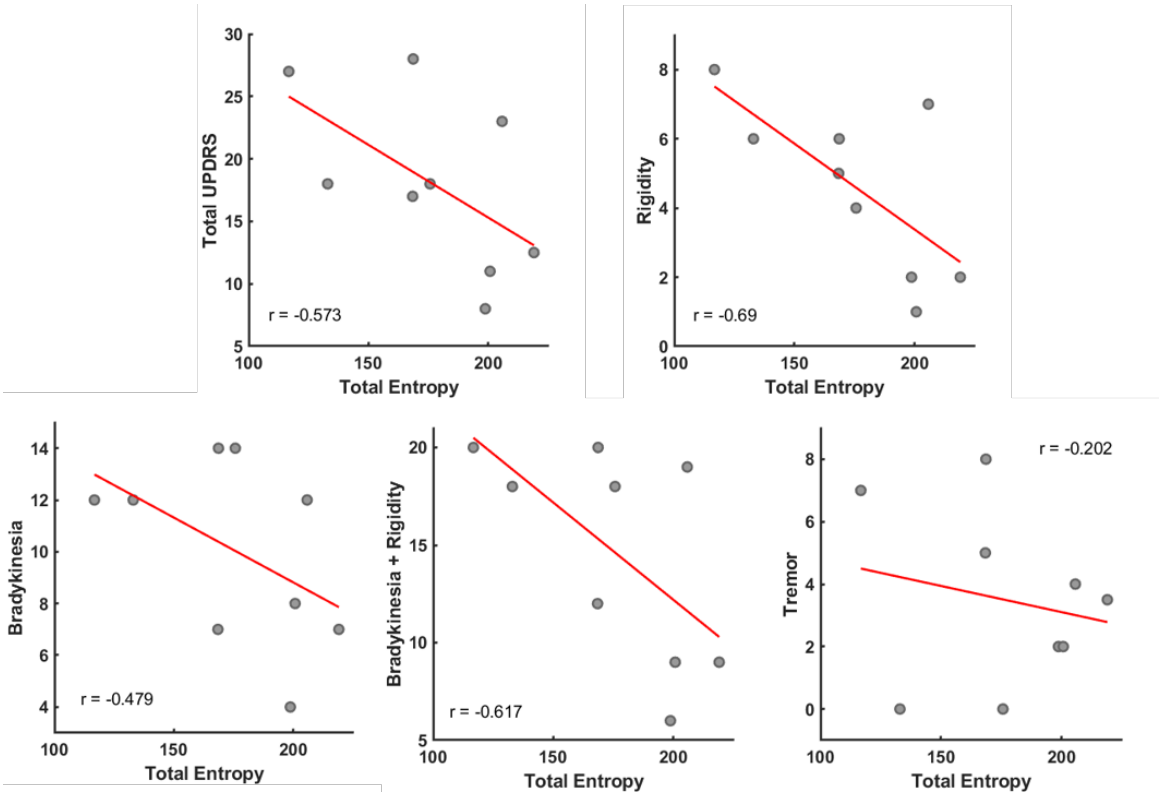

Figure 4. 40: Clinical scores and the sum of the entropy from all segments from the first off state were used. Total UPDRS scores were correlated to total entropy (r=-0.573, p=0.11), rigidity (r=-0.69, p=0.04), bradykinesia (r=-0.479, p=0.2), bradykinesia plus rigidity (r=-0.617, p=0.08), and tremor (r=-0.202, p=0.6).

CHAPTER V

DISCUSSION AND FUTURE DIRECTIONS

5.1 DISCUSSION

In this research study, we introduced a novel method for the detection of beta bursts using an adaptive segmentation algorithm. We tested three types of adaptive segmentation algorithms on synthetic signals and compared segments to determine ideal performance. We then concluded that nondyadic adaptive segmentation was the optimal choice based on how the artificial beta bursts were detected as a whole, and not truncated as they were with the two other segmentation techniques. The nondyadic segmentation approach was applied to the STN LFP recordings of PD patients, which segmented the data into various lengths.

The segments were binned into six different time windows; there was a higher (0.125s) percentage of smaller segments during the ON state, while larger ($\geq$ 1s) segments were found during the OFF state. A previous study filtered the LFP data around the individual's beta peak frequency, and a threshold was used to detect bursts that are $\geq$ 100ms [Tinkhauser et al., 2017]. In this study, it was crucial to let the algorithm have a broader frequency range to segment the data rather than solely restricting it within a specific beta range. Therefore, high-pass filtering of

the data above 8 Hz introduced more segmentation flexibility into the algorithm and allowed for the detection of smaller segments (125ms). Consequently, the mean entropy of these segments minimized as the segment size increased during the OFF state. On the other hand, less detection of beta oscillations during the ON state caused the mean entropy of the segments to increase.

Tinkhauser's method relied on the amplitude of the signal to detect beta bursts, failing to acknowledge the various characteristics of a burst [Tinkhauser et al., 2017]. However, in this study, an adaptive method which implements entropy minimization was used to detect beta bursts and segment the LFP bases on the consistency of the spectrum along the time axis. Additionally, more than one burst characteristic was considered, such as entropy minimization, normalized beta power, and beta power ratio. These characteristics helped determine the modulation of larger bursts by beta-band activity. Consequently, the normalization of beta band power to its segment length confirmed the presence of beta oscillations in all segment bins. Moreover, segments normalized to the maximum beta power were positively correlated to an increasing segment size while shifting from low-beta (OFF state) to high-beta (ON state) relating this to the pathological part of the disease.

Patient improvement and efficacy of the medication were confirmed by the significant difference that was observed in keyboard and mUPDRS scores; Keyboard scores improved in the ON states while mUPDRS scores decreased. Tinkhauser et al., 2017, correlated the percentage of bursts $\geq$ 0.5s ($r=-0.5$, $p=0.45$) and $<$ 0.5s ($r=0.5$, $p=0.45$) with mUPDRS; here, the difference in entropy for resting state data was correlated to the clinical scores obtained, and the correlation was higher and significant for Δ mUPDRS ($r=-0.825$, $p<0.001$), keyboard improvement (%) ($r=-0.80$, $p<0.001$), Δ bradykinesia ($r=-0.727$, $p<0.001$) scores . Furthermore, the previous study also reported that the correlation between segment size and clinical improvement became positive

once bursts length reached at least 0.5s [Tinkhauser et al., 2017]. However, in this study correlation improved once the segments length reached 375ms, signifying that beta oscillations with a duration of ≥ 375ms may be the pathological ones correlating with PD symptoms. In addition, the computer-based keyboard scores ($r=-0.800$, $p<0.001$) were found to be more insightful than the bradykinesia scores ($r=-0.727$, $p<0.001$) because they had a stronger correlation with the difference in weighted entropy. The same phenomenon was found for segments ≥ 1s when correlating the difference in unweighted entropy with keyboard scores ($r=-0.734$, $p<0.001$), and bradykinesia scores ($r=-0.615$, $p<0.001$). Based on these findings, we hypothesize that smaller segments do not contribute to clinical impairment as much as larger segments do. As a result, making larger beta bursts the target for adaptive DBS might reduce symptom impairment even further.

Eusebio et al., 2012 reviews the evidence supporting the DBS suppression of pathological beta activity and concludes that suppression of excessive beta synchrony is responsible for motor improvement. However, in this work, the full beta-band was divided into two subcategories, low and high beta, which helped determine which segments were predominantly associated with clinical impairment. It was found that as the length of the segmentation increased, the energy of low-beta bursts also increased. Based on this observation, in each segment the energy ratio of low beta to high beta band was calculated and this ratio was used to weigh the entropy of the segments. As it has been noted in Figure 4.11B, there is a possibility that patients may experience low-beta bursts within a specific range because of the fluctuation seen on the weighted keyboard improvement correlation curve. For that reason, using a unique low-beta range for each patient could improve the weighed correlation for each segment bin. Additionally, full beta and low-beta band power was correlated with keyboard and UPDRS scores, supporting

the findings of Ozturk et al., 2019. Lastly, entropy gain helped establish baseline correlations determining it to be most correlated with total UPDRS than with individual sub-sections.

Weighing the normalized entropy of each segment with its corresponding power ratio helped highlight the significant impact beta bursts have on patient impairment. It was noted for all MDS-UPDRS, keyboard, and bradykinesia scores, the correlation was higher when a weighted entropy based on low/high beta band ratio was used. However, the adaptive segmentation algorithm is limited to specific segmentation time windows but if more flexibility were achieved, a better understanding will be gained about how beta bursts affect PD patients. Overall, the use of this algorithm can help establish a different type of method for the detection of beta bursts and not limit burst detection to the one currently used today.

5.2 FUTURE DIRECTIONS

Based on the fact that 120s pre-recorded resting data was used, the burst detection algorithm presented would need to be tested on longer LFP recordings of freely moving patients. Moreover, in clinical practice the entropy of beta bursts might serve as a better biomarker for the quantification of disease severity and improvement, than the amplitude of the bursts alone. Based on the results obtained from keyboard and bradykinesia scores, we argue that such method should be coupled with computer based objective measurement for motor symptoms of the disease as our results show a stronger correlation between neural data and keyboard scores. Finally, the entropy of adaptively segmented beta bursts could be used as a feedback signal in adaptive DBS scenarios.

REFERENCES

Abosch, A., Lanctin, D., Onaran, I., Eberly, L., Spaniol, M., & Ince, N. F. (2012). Long-term Recordings of Local Field Potentials From Implanted Deep Brain Stimulation Electrodes. *Neurosurgery,71*(4), 804-814. doi:10.1227/neu.0b013e3182676b91

Boulet, B. (2014). *Fundamentals of Signals and Systems*. Boston: Course Technology.

Bouthour, W., Mégevand, P., Donoghue, J., Lüscher, C., Birbaumer, N., & Krack, P. (2019). Author Correction: Biomarkers for closed-loop deep brain stimulation in Parkinson disease and beyond. *Nature Reviews Neurology, 15*(6), 363–363. doi: 10.1038/s41582-019-0189-x

Brown, P., & Williams, D. (2005). Basal ganglia local field potential activity: Character and functional significance in the human. *Clinical Neurophysiology, 116*(11), 2510–2519. doi: 10.1016/j.clinph.2005.05.009

Coffey, R. J. (2009). Deep Brain Stimulation Devices: A Brief Technical History and Review. *Artificial Organs, 33*(3), 208–220. doi: 10.1111/j.1525-1594.2008.00620.x

Coifman, R., & Wickerhauser, M. (1992). Entropy-based algorithms for best basis selection. *IEEE Transactions on Information Theory, 38*(2), 713–718. doi: 10.1109/18.119732

Darvas, F., & Hebb, A. O. (2014). Task specific inter-hemispheric coupling in human subthalamic nuclei. *Frontiers in Human Neuroscience, 8*. doi: 10.3389/fnhum.2014.00701

Eusebio, A., Cagnan, H., & Brown, P. (2012). Does suppression of oscillatory

synchronisation mediate some of the therapeutic effects of DBS in patients with Parkinson's disease? *Frontiers in Integrative Neuroscience,6*. doi:10.3389/fnint.2012.00047

Eusebio, A., Thevathasan, W., Doyle Gaynor, L., Pogosyan, A., Bye, E., Foltynie, T., Zrinzo, L., Ashkan, K., Aziz, T., & Brown, P. (2011). Deep brain stimulation can suppress pathological synchronisation in parkinsonian patients. *Journal of neurology, neurosurgery, and psychiatry*, *82*(5), 569–573. https://doi.org/10.1136/jnnp.2010.217489

Fang, J. Y., & Tolleson, C. (2017). The role of deep brain stimulation in Parkinson's disease: An overview and update on new developments. *Neuropsychiatric Disease and Treatment, Volume 13*, 723-732. doi:10.2147/ndt.s113998

Goedert, M., & Compston, A. (2017). Parkinsons disease — the story of an eponym. *Nature Reviews Neurology, 14*(1), 57-62. doi:10.1038/nrneurol.2017.165

Goetz, C. G., Tilley, B. C., Shaftman, S. R., Stebbins, G. T., Fahn, S., Martinez-Martin, P., Lapelle, N. (2008). Movement Disorder Society-sponsored revision of the Unified Parkinsons Disease Rating Scale (MDS-UPDRS): Scale presentation and clinimetric testing results. *Movement Disorders, 23(15), 2129–2170*. doi: 10.1002/mds.22340

Hickey, P., & Stacy, M. (2016). Deep Brain Stimulation: A Paradigm Shifting Approach to Treat Parkinson's Disease. *Frontiers in Neuroscience, 10*. doi: 10.3389/fnins.2016.00173

Ince, N. F., & Abosch, A. (2014). Clinical Implications of Local Field Potentials for Understanding and Treating Movement Disorders. *Stereotactic and Functional Neurosurgery,92*(4), 251-263. doi:10.1159/000364913

Ince, N. F., & Arica, S. (2004). Analysis and visualization of ERD and ERS with adapted local

cosine transforms. *The 26th Annual International Conference of the IEEE Engineering in Medicine and Biology Society*. doi: 10.1109/iembs.2004.1403152

Ince, N. F., Arica, S., & Tewfik, A. (2006). Classification of single trial motor imagery EEG recordings with subject adapted nondyadic arbitrary time-frequency tilings. *Journal of Neural Engineering, 3*(3), 235–244. doi: 10.1088/1741-2560/3/3/006

Ince, N., Arica, S., & Tewfik, A. (2006). Using Multiresolution Space-Time-Frequency Features for the Classification Motor Imagery EEG Recordings in a Brain Computer Interface Task. *2006 16th IEEE Signal Processing Society Workshop on Machine Learning for Signal Processing.* doi: 10.1109/mlsp.2006.275575

Ince, N. F., Goksu, F., Tewfik, A. H., & Arica, S. (2009). Adapting subject specific motor imagery EEG patterns in space-time-frequency for a brain computer interface. *Biomedical Signal Processing and Control, 4*(3), 236–246. doi: 10.1016/j.bspc.2009.03.005

Ince, N. F., Gupte, A., Wichmann, T., Ashe, J., Henry, T., Bebler, M., Eberly, L., Abosch, A. (2010). Selection of Optimal Programming Contacts Based on Local Field Potential Recordings From Subthalamic Nucleus in Patients With Parkinson's Disease. *Neurosurgery,67*(2), 390-397. doi:10.1227/01.neu.0000372091.64824.63

Ince, N. F., Tewfik, A. H., & Arica, S. (2007). Extraction subject-specific motor imagery time–frequency patterns for single trial EEG classification. *Computers in Biology and Medicine, 37*(4), 499–508. doi: 10.1016/j.compbiomed.2006.08.014

Jankovic, J. (2008). Parkinson’s disease: clinical features and diagnosis. *Journal of Neurology, Neurosurgery & Psychiatry*, 79(4), 368–376. doi: 10.1136/jnnp.2007.131045

Jiang, T., Siddiqui, H., Ray, S., Asman, P., Ozturk, M., & Ince, N. F. (2017). A portable platform

to collect and review behavioral data simultaneously with neurophysiological signals. *2017 39th Annual International Conference of the IEEE Engineering in Medicine and Biology Society (EMBC)*. doi:10.1109/embc.2017.8037190

Kühn, A. A., Kupsch, A., Schneider, G.-H., & Brown, P. (2006). Reduction in subthalamic 8-35 Hz oscillatory activity correlates with clinical improvement in Parkinson's disease. *European Journal of Neuroscience, 23(7)*, 1956–1960. doi: 10.1111/j.1460-9568.2006.04717.x

Mallat, S. G., & Peyré Gabriel. (2009). *A wavelet tour of signal processing: The Sparse Way.* Amsterdam: Elsevier /Academic Press.

Mayfield Brain & Spine. (2018, April). Parkinson's Disease (PD). Retrieved March 20, 2020, from https://mayfieldclinic.com/pe-pd.htm

Meloni, G. (2015, August 1). Space and Time Frequency-Dependent Interactions in Subthalamic Nucleus Local Field Potentials in Parkinson's Disease (Master's Thesis, University of Houston). Retrieved from http://hdl.handle.net/10657/1983

Naqvi, E. (2018, August 6). Parkinson's Disease Statistics. Retrieved March 23, 2020, from https://parkinsonsnewstoday.com/parkinsons-disease-statistics/

Ozturk, M., Abosch, A., Francis, D., Wu, J., Jimenez-Shahed, J., & Ince, N. F. (2019). Distinct Subthalamic Coupling in the ON State Describes Motor Performance in Parkinson's Disease. *Movement Disorders, 35*(1), 91–100. doi: 10.1002/mds.27800

Parkinson, J. (1969). An Essay On The Shaking Palsy. *Archives of Neurology, 20*(4), 441–445. doi: 10.1001/archneur.1969.00480100117017

Perlmutter, J. S. (2009). Assessment of Parkinson Disease Manifestations. *Current Protocols in Neuroscience*, 49(1). doi: 10.1002/0471142301.ns1001s49

Reeve, A., Simcox, E., & Turnbull, D. (2014). Ageing and Parkinson's disease: Why is advancing age the biggest risk factor? *Ageing Research Reviews, 14,* 19–30. doi: 10.1016/j.arr.2014.01.004

Saito, N., Coifman, R. R., Geshwind, F. B., & Warner, F. (2002). Discriminant feature extraction using empirical probability density estimation and a local basis library. *Pattern Recognition, 35*(12), 2841–2852. doi: 10.1016/s0031-3203(02)00019-5

Salat, D., & Tolosa, E. (2013). Levodopa in the Treatment of Parkinson's Disease: Current Status and New Developments. *Journal of Parkinson's Disease, 3, 255–269*. doi: 10.3233/JPD-130186

Thompson, J. A., Lanctin, D., Ince, N. F., & Abosch, A. (2014). Clinical Implications of Local Field Potentials for Understanding and Treating Movement Disorders. *Stereotactic and Functional Neurosurgery, 92*(4), 251–263. doi: 10.1159/000364913

Tinkhauser, G., Pogosyan, A., Little, S., Beudel, M., Herz, D. M., Tan, H., & Brown, P. (2017). The modulatory effect of adaptive deep brain stimulation on beta bursts in Parkinson's disease. *Brain: a journal of neurology*, *140*(4), 1053–1067. https://doi.org/10.1093/brain/awx010

Tinkhauser, G., Pogosyan, A., Tan, H., Herz, D. M., Kühn, A. A., & Brown, P. (2017). Beta burst dynamics in Parkinson's disease OFF and ON dopaminergic medication. *Brain,140*(11), 2968-2981. doi:10.1093/brain/awx252

Tinkhauser, G., Torrecillos, F., Duclos, Y., Tan, H., Pogosyan, A., Fischer, P., Carron R., Welter M., Karachi C., Vandenberghe W., Nuttin B., Witjas T., Regis J., Azulay J., Eusebio A., Brown, P. (2018). Beta burst coupling across the motor circuit in Parkinson's disease. *Neurobiology of Disease, 117*, 217–225. doi: 10.1016/j.nbd.2018.06.007

Wagle Shukla, A., & Okun, M. S. (2014). Surgical treatment of Parkinson's disease: patients, targets, devices, and approaches. *Neurotherapeutics: the journal of the American Society for Experimental NeuroTherapeutics*, *11*(1), 47–59. https://doi.org/10.1007/s13311-013-235-0

Wichmann, T., & Delong, M. R. (2006). Deep Brain Stimulation for Neurologic and Neuropsychiatric Disorders. *Neuron*, 52(1), 197–204. doi: 10.1016/j.neuron.2006.09.02

Wichmann, T., & Dostrovsky, J. (2011). Pathological basal ganglia activity in movement disorders. *Neuroscience,198*, 232-244. doi:10.1016/j.neuroscience.2011.06.048